Title:

Alzheimer's disease pathogenesis is dependent on neuronal receptor PTPσ

Authors:

Yuanzheng Gu[1], Yaoling Shu[1], Angela W. Corona[2], Kui Xu[1§], Allen F. Yi[1], Shannon Chen[1], Man Luo[1†], Michel L. Tremblay[3], Gary E. Landreth[2], Randy J. Nelson[1], Jerry Silver[2], Yingjie Shen[1*]

Affiliation:

[1]Department of Neuroscience, Neuroscience Research Institute, The Ohio State University Wexner Medical Center, 460 West 12th Ave, Columbus, OH 43210, USA.

[2]Case Western Reserve University. 10900 Euclid Ave, Cleveland, OH 44106

[§]Current address: Division of Neurosurgery, Cincinnati Children's Hospital Medical Center, 3333 Burnet Ave, Cincinnati, OH 45229, USA.

[†]Current address: Department of Biostatistics, School of Public Health, Boston University, 715 Albany St, Boston, MA 02118, USA.

[3]Department of Biochemistry and Goodman Cancer Research Centre, McGill University, 1160 Avenue des Pins, Montréal, Quebec, Canada H3A 1A3.

*Correspondence to: yingjie.shen@osumc.edu

Acknowledgements We thank Dennis Selkoe, Jared Cregg, and Miriam Osterfield for scientific discussion; John Flanagan for facilitating study prior to this work; Anthony Brown, Christopher Edwards, Bradley Lang, Patricia Hess, Yan Wang for comments on the manuscript; Jonathan Cherry for technical support on imaging; Li Zhang for technical advice on rodent pathology. The behavioral data were collected with the support of National Institute of Neurological Disorders and Stroke Grant P30 NS045758. Aβ ELISA analyses were performed with the support of R01 AG043522-01 to Landreth (PI) by National Institutes of Health. The rest of the work was supported by Ohio State University Startup Funds to Shen (PI).

Author contributions YG, YS, AWC, KX, AFY, SC, and ML conducted experiments and data analyses, under the supervision of GEL, RJN, and Y Shen. YG, KX, and AWC also provided comments on the manuscript. MLT provided PTPσ-deficient mice and comments on the manuscript. JS, GEL, and RJN advised on experimental design and commented on the manuscript. Y Shen conceived the project, designed the study, and wrote the paper.

Author Information Reprints and permissions information is available at www.nature.com/reprints. The authors declare no competing financial interests. Readers are welcome to comment on the online version of the paper. Correspondence and requests for materials should be addressed to Y Shen (yingjie.shen@osumc.edu).

Note: as there are 2 authors whose initials are YS, the last author is noted as "Y Shen".

Title:

Alzheimer's disease pathogenesis is dependent on neuronal receptor PTPσ

Abstract:

β-amyloid accumulation and Tau aggregation are hallmarks of Alzheimer's disease, yet their underlying molecular mechanisms remain obscure, hindering therapeutic advances. Here we report that neuronal receptor PTPσ mediates both β-amyloid and Tau pathogenesis in two mouse models. In the brain, PTPσ binds to β-amyloid precursor protein (APP). Depletion of PTPσ reduces the affinity between APP and β-secretase, diminishing APP proteolytic products by β- and γ-cleavage without affecting other major substrates of the secretases, suggesting a specificity of β-amyloidogenic regulation. In human APP transgenic mice during aging, the progression of β-amyloidosis, Tau aggregation, neuroinflammation, synaptic loss, as well as behavioral deficits, all show unambiguous dependency on the expression of PTPσ. Additionally, the aggregates of endogenous Tau are found in a distribution pattern similar to that of early stage neurofibrillary tangles in Alzheimer brains. Together, these findings unveil a gatekeeping role of PTPσ upstream of the degenerative pathogenesis, indicating a potential for this neuronal receptor as a drug target for Alzheimer's disease.

Main Text:

A definitive pathological hallmark of Alzheimer's disease (AD) is the progressive aggregation of β-amyloid (Aβ) peptides in the brain, a process also known as β-amyloidosis, which is often accompanied by neuroinflammation and formation of neurofibrillary tangles containing Tau, a microtubule binding protein.

Although the etiological mechanisms of AD have been an ongoing debate, concrete evidence from human genetic studies showed that overproduction of Aβ due to gene mutations inevitably inflicts cascades of cytotoxic events, ultimately leading to neurodegeneration and decay of brain functions. Accumulation of Aβ peptides, especially in their soluble forms, is therefore recognized as a key culprit in the development of AD [1]. In the brain, Aβ peptides mainly derive from sequential cleavage of neuronal amyloid precursor protein (APP) by the β- and γ-secretases. However, despite decades of research, molecular regulation of the amyloidogenic secretase activities remains poorly understood, hindering the design of therapeutics to specifically target the APP amyloidogenic pathway.

Pharmacological inhibition of the β- and γ-secretase activities, although effective in suppressing Aβ production, interferes with physiological function of the secretases on their other substrates. Such intervention strategies therefore are often innately associated with untoward side effects, which have led to several failed clinical trials in the past [2-4]. To date, no therapeutic regimen is available to prevent the onset of AD or curtail its progression.

Here we report our findings that identify neuronal receptor PTPσ (protein tyrosine phosphatase sigma) as a potential molecular target to curb Aβ pathogenesis. Genetic

depletion of PTPσ lowers β-secretase affinity to APP and suppresses Aβ accumulation in a specific manner that does not generically inhibit β- and γ-secretase activities.

Besides Aβ, Tau is another biomarker that has been intensively studied in AD. Cognitive decline in patients often correlates better with Tau pathology than with Aβ burden [5,6]. Overwhelming evidence also substantiated that malfunction of Tau contributes to synaptic loss and neuronal deterioration [7]. However, what triggers the pathological changes of Tau in AD remains a mystery. Whether neurotoxic Aβ can lead to Tau pathology *in vivo* has been a debate since quintessential neurofibrillary Tau tangles have not been reported in any of the APP transgenic mouse models, even in those with severe cerebral β-amyloidosis. Here we show that during the process of aging, Tau aggregates form in the brains of two APP transgenic mouse models with a similar distribution pattern as seen in postmortem AD brains, suggesting that Tau misfolding can develop as an event downstream from the expression of amyloidogenic APP transgenes. Genetic depletion of PTPσ, which suppresses Aβ accumulation, also inhibits the aggregation of Tau.

In the two mouse models we studied, a spectrum of AD neuropathologies and behavioral deficits all demonstrate a clear dependency on PTPσ, indicating that this neuronal receptor is a pivotal upstream player in AD pathogenesis.

PTPσ is an APP binding partner in the brain.

Previously identified as a neuronal receptor of extracellular proteoglycans [8-10], PTPσ is expressed throughout the adult nervous system, most predominantly in the hippocampus [11,12], one of earliest affected brain regions in AD. Using

immunohistochemistry and confocal imaging, we found that PTPσ and APP (the precursor of Aβ) colocalize in hippocampal pyramidal neurons of adult rat brains, most intensively in the initial segments of apical dendrites, and in the perinuclear and axonal regions with a punctate pattern (Fig. 1a-f). To assess whether this colocalization reflects a binding interaction between these two molecules, we tested their co-immunoprecipitation from brain homogenates. In brains of rats and mice with different genetic background, using various antibodies of APP and PTPσ, we consistently detected a fraction of PTPσ that co-immunoprecipitates with APP, providing evidence of a molecular complex between these two transmembrane proteins (Fig. 1h, i; Extended Data Fig. 1).

Genetic depletion of PTPσ reduces β-amyloidogenic products of APP.

The molecular interaction between PTPσ and APP prompted us to investigate whether PTPσ plays a role in amyloidogenic processing of APP. In neurons, APP is mainly processed through alternative cleavage by either α- or β-secretase. These secretases release the N-terminal portion of APP from its membrane-tethering C-terminal fragment (CTFα or CTFβ, respectively), which can be further processed by the γ-secretase [13,14]. Sequential cleavage of APP by the β- and γ-secretases is regarded as amyloidogenic processing since it produces Aβ peptides [15]. When overproduced, the Aβ peptides can form soluble oligomers that trigger ramification of cytotoxic cascades, whereas progressive aggregation of Aβ eventually results in the formation of senile plaques in the brains of AD patients (Fig. 2a). To test the effect of PTPσ in this amyloidogenic processing, we analyzed the levels of APP β- and γ-cleavage products in mouse brains with or without PTPσ.

Western blot analysis with protein extracts from mouse brains showed that genetic depletion of PTPσ does not affect the expression level of full length APP (Fig. 2b; Extended Data Fig 2a). However, an antibody against the C-terminus of APP detects a band at a molecular weight consistent with CTFβ, which is reduced in PTPσ-deficient mice as compared to their age- sex-matched wild type littermates (Fig. 2b). Additionally, in two AD mouse models expressing human APP genes with amyloidogenic mutations [16,17], we observed a similar decrease of an APP CTF upon PTPσ depletion (Fig. 2b; Extended Data Fig. 2b). The TgAPP-SwDI and TgAPP-SwInd mice, each expressing a human APP transgene harboring the Swedish mutation near the β-cleavage site, were crossed with the PTPσ line to generate offsprings that are heterozygous for their respective APP transgene, with or without PTPσ. Because the Swedish mutation carried by these APP transgenes is prone to β-cleavage, the predominant form of APP CTF in these transgenic mice is predicted to be CTFβ. Thus, the reduction of APP CTF in PTPσ-deficient APP transgenic mice may indicate a regulatory role of PTPσ on CTFβ level. However, since the APP C-terminal antibody used in these experiments can recognize both CTFα and CTFβ, as well as the phosphorylated species of these CTFs (longer exposure of western blots showed multiple CTF bands), judging the identity of the reduced CTF simply by its molecular weight may be inadequate. We therefore performed CTFβ immunopurification with subsequent western blot detection, using an antibody that recognizes CTFβ but not CTFα (Fig. 2c, d; Extended Data Fig. 2c, d). With this definitive method, we confirmed that PTPσ depletion decreases the level of CTFβ originated from both mouse endogenous and human transgenic APP.

Because CTFβ is an intermediate proteolytic product between β- and γ-cleavage, its decreased steady state level could result from either reduced production by β-cleavage or increased degradation by subsequent γ-secretase cleavage (Fig. 2a). To distinguish between these two possibilities, we measured the level of Aβ peptides, which are downstream products from CTFβ degradation by γ-cleavage. Using ELISA assays with brain homogenates from the TgAPP-SwDI mice, we found that PTPσ depletion decreases the levels of Aβ peptides to a similar degree as that of CTFβ (Fig. 2e, f). Consistently, as Aβ peptides gradually aggregate into plaques during aging of the transgenic mice, we observed a substantial decrease of cerebral Aβ deposition in APP transgenic PTPσ-deficient mice as compared to the age-matched APP transgenic littermates expressing wild type PTPσ (Fig. 2g, h; Extended Data Fig. 2e, f). Thus, the concurrent decrease of β- and γ-cleavage products argues against an increased γ-secretase activity, but instead suggests a reduced β-secretase cleavage of APP, which suppresses not only the level of CTFβ but also downstream Aβ production in PTPσ-deficient brains.

Curtailed progression of β-amyloidosis in the absence of PTPσ.

Progressive cerebral Aβ aggregation (β-amyloidosis) is regarded as a benchmark of AD progression. To investigate the effects of PTPσ on this pathological development, we monitored Aβ deposits in the brains of 9-month old (mid-aged) and 16-month old (aged) TgAPP-SwDI mice. At 9 months of age, Aβ deposits are found predominantly in the hippocampus, especially in the hilus of the dentate gyrus (DG) (Fig. 2g, h). By 16 months, the pathology spreads massively throughout the entire brain. The propagation of

Aβ deposition, however, is curbed by genetic depletion of PTPσ, as quantified using the DG hilus as a representative area (Fig. 2i). Between the ages of 9 and 16 months, the Aβ burden is more than doubled in TgAPP-SwDI mice expressing wild type PTPσ [APP-SwDI(+)PTPσ(+/+)], but only shows marginal increase in the transgenic mice lacking functional PTPσ [APP-SwDI(+)PTPσ(-/-)]. Meanwhile, the Aβ loads measured in 9-month old APP-SwDI(+)PTPσ(+/+) mice are similar to those of 16-month old APP-SwDI(+)PTPσ(-/-) mice (p=0.95), indicating a restraint of disease progression by PTPσ depletion (Fig. 2i).

Decreased BACE1-APP affinity in PTPσ-deficient brains.

Consistent with these observations that suggest a facilitating role of PTPσ in APP β-cleavage, our data further reveal that PTPσ depletion weakens the interaction of APP with BACE1, the β-secretase in the brain. To test the *in vivo* affinity between BACE1 and APP, we performed co-immunoprecipitation of the enzyme and substrate from mouse brain homogenates in buffers with serially increased detergent stringency. Whereas BACE1-APP association is nearly equal in wild type and PTPσ-deficient brains under mild buffer conditions, increasing detergent stringency in the buffer unveils that the molecular complex is more vulnerable to dissociation in brains without PTPσ (Fig. 3). Thus a lower BACE1-APP affinity in PTPσ-deficient brains may likely be an underlying mechanism for the decreased levels of CTFβ and its derivative Aβ.

Although it cannot be ruled out that some alternative uncharacterized pathway may contribute to the parallel decrease of CTFβ and Aβ in PTPσ-deficient brains, these

data consistently support the notion that PTPσ regulates APP amyloidogenic processing, likely via facilitation of BACE1 activity on APP, the initial process of Aβ production.

The specificity of β-amyloidogenic regulation by PTPσ.

The constraining effect of PTPσ on APP amyloidogenic products led us to further question whether this observation reflects a specific regulation of APP metabolism, or alternatively, a general modulation on the β- and γ-secretases. We first assessed the expression level of these secretases in mouse brains with or without PTPσ, and found no change for BACE1 or the essential subunits of γ-secretase (Fig. 4a, b). Additionally, we tested whether PTPσ broadly modulates β- and γ-secretase activities, by examining the proteolytic processing of their other substrates. Besides APP, Neuregulin1 (NRG1) [18-20] and Notch [21-23] are the major *in vivo* substrates of BACE1 and γ-secretase, respectively. Neither BACE1 cleavage of NRG1 nor γ-secretase cleavage of Notch is affected by PTPσ deficiency (Fig. 4c, d). Taken together, these data rule out a generic modulation of β- and γ-secretases, but rather suggest a specificity of APP amyloidogenic regulation by PTPσ.

PTPσ depletion relieves neuroinflammation and synaptic impairment in APP transgenic mice.

Substantial evidence from earlier studies has established that overproduction of Aβ in the brain elicits multiplex downstream pathological events, including chronic inflammatory responses of the glia, such as persistent astrogliosis. The reactive

(inflammatory) glia would then crosstalk with neurons, evoking a vicious feedback loop that amplifies neurodegeneration during disease progression [24-26].

The TgAPP-SwDI model is one of the earliest to develop neurodegenerative pathologies and behavioral deficits among many existing AD mouse models [16]. We therefore chose these mice to further examine the role of PTPσ in AD pathologies downstream of neurotoxic Aβ.

The APP-SwDI(+)PTPσ(+/+) mice, which express the TgAPP-SwDI transgene and wild type PTPσ, have developed severe neuroinflammation in the brain by the age of 9 months, as measured by the level of GFAP (glial fibrillary acidic protein), a marker of astrogliosis (Extended Data Fig. 3). In the DG hilus, for example, GFAP expression level in the APP-SwDI(+)PTPσ(+/+) mice is more than tenfold compared to that in age-matched non-transgenic littermates [APP-SwDI(-)PTPσ(+/+)] (Extended Data Fig. 3b). PTPσ deficiency, however, effectively attenuates astrogliosis induced by the amyloidogenic transgene. In the APP-SwDI(+)PTPσ(-/-) brains, depletion of PTPσ restores GFAP expression back to a level close to that of non-transgenic wild type littermates (Extended Data Fig. 3b).

Among all brain regions, the most affected by the expression of TgAPP-SwDI transgene appears to be the hilus of the DG, where Aβ deposition and astrogliosis are both found to be the most severe (Fig. 2g, h; Extended Data Fig. 3). We therefore questioned whether the pathologies in this area have an impact on the mossy fiber axons of DG pyramidal neurons, which project through the hilus into the CA3 region, where they synapse with the CA3 dendrites. Upon examining the presynaptic markers in CA3 mossy fiber terminal zone, we found decreased levels of Synaptophysin and Synapsin-1

in the APP-SwDI(+)PTPσ(+/+) mice, comparing to their age-matched non-transgenic littermates (Extended Data Fig. 4, data not shown for Synapsin-1). Such synaptic impairment, evidently resulting from the expression of the APP transgene and possibly the overproduction of Aβ, is reversed by genetic depletion of PTPσ in the APP-SwDI(+)PTPσ(-/-) mice (Extended Data Fig. 4).

Interestingly, we noticed that the APP-SwDI(+)PTPσ(-/-) mice sometimes express higher levels of presynaptic markers in the CA3 terminal zone than their age-matched non-transgenic wild type littermates (Extended Data Fig. 4g). This observation, although not statistically significant in our quantification analysis, may suggest an additional synaptic effect of PTPσ that is independent of the APP transgene, as observed in previous studies [27].

Tau pathology in aging AD mouse brains is dependent on PTPσ.

Neurofibrillary tangles composed of hyperphosphorylated and aggregated Tau are commonly found in AD brains. These tangles tend to develop in a hierarchical pattern, appearing first in the entorhinal cortex before spreading to other brain regions [5,6]. The precise mechanism of tangle formation, however, is poorly understood. The fact that Tau tangles and Aβ deposits can be found in separate locations in postmortem brains has led to the question of whether Tau pathology in AD is independent of Aβ accumulation [5,6]. Additionally, despite severe cerebral β-amyloidosis in many APP transgenic mouse models, Tau tangles have not been reported, further questioning the relationship between Aβ and Tau pathologies *in vivo*.

Nonetheless, a few studies did show non-tangle like assemblies of Tau in dystrophic neurites surrounding Aβ plaques in APP transgenic mouse lines [28-30], arguing that Aβ can be a causal factor for Tau dysregulation, despite that the precise nature of Tau pathologies may be different between human and mouse. In our histological analysis using an antibody against the proline-rich domain of Tau, we observed Tau aggregation in the brains of both TgAPP-SwDI and TgAPP-SwInd mice during the course of aging (around 9 months for the both the APP-SwDI(+)PTPσ(+/+) mice and 15 months for the APP-SwInd(+)PTPσ(+/+) mice) (Fig. 5; Extended Data Fig. 5). Such aggregation is not seen in aged-matched non-transgenic littermates (Fig. 5h), suggesting that it is a pathological event downstream from the expression of amyloidogenic APP transgenes, possibly a result of Aβ cytotoxicity. Genetic depletion of PTPσ, which diminishes Aβ levels, suppresses Tau aggregation in both TgAPP-SwDI and TgAPP-SwInd mice (Fig. 5; Extended Data Fig. 5).

Upon closer examination, the Tau aggregates are often found in punctate shapes, likely in debris from degenerated cell bodies and neurites, scattered in areas free of nuclear staining (Extended Data Fig. 6a-f). Rarely, a few are in fibrillary structures, probably in degenerated cells before disassembling (Extended Data Extended Data Fig. 6g, h). In both TgAPP-SwDI and TgAPP-SwInd mice, the Tau aggregates are found predominantly in the molecular layer of the piriform and entorhinal cortices, and occasionally in the hippocampal region (Fig. 5; Extended Data Fig. 5), reminiscent of the early stage tangle locations in AD brains [31]. To confirm these findings, we used an additional antibody recognizing the C-terminus of Tau and detected the same morphologies (Extended Data Fig. 6i) and distribution pattern (Fig. 5a).

Consistent with the findings in postmortem AD brains, the distribution pattern of Tau aggregates in the TgAPP-SwDI brain does not correlate with that of Aβ deposition, which is pronounced in the hippocampus yet barely detectable in the piriform or entorhinal cortex at the age of 9 months (Fig. 2g, h). Given that the causation of Tau pathology in these mice is possibly related to the overproduced Aβ, the segregation of Aβ and Tau depositions in different brain regions may indicate that the cytotoxicity originates from soluble Aβ instead of the deposited amyloid. It is also evident that neurons in different brain regions are not equally vulnerable to developing Tau pathology.

We next examined whether the expression of APP transgenes or genetic depletion of PTPσ regulates Tau aggregation by changing its expression level and/or phosphorylation status. Western blot analysis of brain homogenates showed that Tau protein expression is not affected by the APP transgenes or PTPσ (Extended Data Fig. 7), suggesting that the aggregation may be due to local misfolding of Tau rather than an overexpression of this protein. Moreover, the TgAPP-SwDI or TgAPP-SwInd transgene, which apparently causes Tau aggregation, does not enhance the phosphorylation of Tau residues including Serine191, Therionine194, and Therionine220 (data not shown), whose homologues in human Tau (Serine202, Therionine205, and Therionine231) are typically hyperphosphorylated in neurofibrillary tangles. These findings are consistent with a recent quantitative study showing similar post-translational modifications in wild type and TgAPP-SwInd mice [32]. Furthermore, unlike previously reported [28,29], we could not detect these phosphorylated residues in the Tau aggregates, suggesting that the epitopes are either missing (residues not phosphorylated or cleaved off) or embedded

inside the misfolding. Given the complexity of Tau post-translational modification, one cannot rule out that the aggregation may be mediated by some unidentified modification(s) of Tau. It is also possible that other factors, such as molecules that bind to Tau, may precipitate the aggregation.

Although the underlying mechanism is still unclear, our finding of Tau pathology in these mice establishes a causal link between the expression of amyloidogenic APP transgenes and a dysregulation of Tau assembly. Our data also suggest a possibility that PTPσ depletion may suppress tau aggregation by reducing amyloidogenic products of APP.

Malfunction of Tau is broadly recognized as a neurodegenerative marker since it indicates microtubule deterioration [7]. The constraining effect on Tau aggregation by genetic depletion of PTPσ thus provides additional evidence for the role of this receptor as a pivotal regulator of neuronal integrity.

PTPσ deficiency rescues behavioral deficits in AD mouse models.

We next assessed whether the alleviation of neuropathologies by PTPσ depletion is accompanied with a rescue from AD relevant behavioral deficits. The most common symptoms of AD include short-term memory loss and apathy among the earliest, followed by spatial disorientation amid impairment of many cognitive functions as the dementia progresses. Using Y maze and novel object assays as surrogate models, we evaluated these cognitive and psychiatric features in the TgAPP-SwDI and TgAPP-SwInd mice.

The Y-maze assay, which allows mice to freely explore three identical arms, measures their short-term spatial memory. It is based on the natural tendency of mice to alternate arm exploration without repetitions. The performance is scored by the percentage of spontaneous alternations among total arm entries, and a higher score indicates better spatial navigation. Compared to the non-transgenic wild type mice within the colony, the APP-SwDI(+)PTPσ(+/+) mice show a clear deficit in their performance. Genetic depletion of PTPσ in the APP-SwDI(+)PTPσ(-/-) mice, however, unequivocally restores the cognitive performance back to the level of non-transgenic wild type mice (Fig. 6a, Extended Data Fig. 8).

Apathy, the most common neuropsychiatric symptom reported among individuals with AD, is characterized by a loss of motivation and diminished attention to novelty, and has been increasingly adopted into early diagnosis of preclinical and early prodromal AD [33-35]. Many patients in early stage AD lose attention to novel aspects of their environment despite their ability to identify novel stimuli, suggesting an underlying defect in the circuitry responsible for further processing of the novel information [33,34]. As a key feature of apathy, such deficits in attention to novelty can be accessed by the "curiosity figures task" or the "oddball task" in patients [33,34,36]. These visual-based novelty encoding tasks are very similar to the novel object assay for rodents, which measures the interest of animals in a novel object (NO) when they are exposed simultaneously to a prefamiliarized object (FO). We therefore used this assay to test the attention to novelty in the APP transgenic mice. When mice are pre-trained to recognize the FO, their attention to novelty is then measured by the discrimination index denoted as the ratio of NO exploration to total object exploration (NO+FO), or alternatively, by the ratio of NO

exploration to FO exploration. Whereas both ratios are commonly used, a combination of these assessments provides a more comprehensive evaluation of animal behavior. In this test, as indicated by both measurements, the expression of APP-SwDI transgene in the APP-SwDI(+)PTPσ(+/+) mice leads to a substantial decrease in NO exploration as compared to non-transgenic wild type mice (Fig. 6b, c; Extended Data Fig. 9). Judging by their NO/FO ratios, it is evident that both the transgenic and non-transgenic groups are able to recognize and differentiate between the two objects (Extended Data Fig. 9a, b). Thus, the reduced NO exploration by the APP-SwDI(+)PTPσ(+/+) mice may reflect a lack of interest in the NO or an inability to shift attention to the NO. Once again, this behavioral deficit is largely reversed by PTPσ deficiency in the APP-SwDI(+)PTPσ(-/-) mice (Fig. 6b, c; Extended Data Fig. 9), consistent with previous observation of increased NO preference in the absence of PTPσ [27].

To further verify the effects of PTPσ on these behavioral aspects, we additionally tested the TgAPP-SwInd mice in both assays and observed similar results, confirming an improvement on both short-term spatial memory and attention to novelty upon genetic depletion of PTPσ (Extended Data Fig. 10).

Discussion

Here we report that β-amyloidosis and several downstream disease features are dependent on PTPσ in two mouse models of genetically inherited AD. This form of AD develops inevitably in people who carry gene mutations that promote amyloidogenic processing of APP and overproduction of Aβ. Our data suggest that targeting PTPσ is a potential therapeutic approach that could overcome such dominant genetic driving forces

to curtail AD progression. The advantage of this targeting strategy is that it suppresses Aβ accumulation without broadly affecting other major substrates of the β- and γ-secretases, thus predicting a more promising translational potential as compared to those in clinical trials that generically inhibit the secretases.

PTPσ was previously characterized as a neuronal receptor of the chondroitin sulfate- and heparan sulfate-proteoglycans (CSPGs and HSPGs) [8,9]. In response to these two classes of extracellular ligands, PTPσ functions as a "molecular switch" by regulating neuronal behavior in opposite manners [10]. Our finding of a pivotal role for the proteoglycan sensor PTPσ in AD pathogenesis may therefore implicate an involvement of the perineuronal matrix in AD etiology.

More than 95% of AD cases are sporadic, which are not genetically inherited but likely result from insults to the brain that occurred earlier in life. AD risk factors, such as traumatic brain injury and cerebral ischemia [37-40], have been shown to induce overproduction of Aβ in both human and rodents [41-45], and speed up progression of this dementia in animal models [46-48]. However, what promotes the amyloidogenic processing of APP in these cases is still a missing piece of the puzzle in understanding the AD-causing effects of these notorious risk factors.

Coincidently, both traumatic brain injury and cerebral ischemia cause pronounced remodeling of the perineuronal microenvironment at lesion sites, marked by increased expression of CSPGs [49-52], a major component of the perineuronal net that is upregulated during neuroinflammation and glial scar formation [53-55]. In the brains of AD patients, CSPGs were found associated with Aβ depositions, further suggesting an uncanny involvement of these proteoglycans in AD development [56]. On the other hand, analogues

of heparan sulfate (HS, carbohydrate side chains of HSPGs that bind to PTPσ) were shown to inhibit BACE1 activity, suggesting their function in preventing Aβ overproduction [57]. After cerebral ischemia, however, the expression of Heparanase, an enzyme that degrades HS, was found markedly increased [58]. Collectively, these findings suggest a disrupted molecular balance between CSPGs and HSPGs in brains after lesion, which may ignite insidious signaling cascades preceding the onset of AD.

We hence speculate upon a mechanism for further study, whereby chronic CSPG upregulation or HSPG degradation in lesioned brains may sustain aberrant signaling through their neuronal sensor PTPσ, leading to biased processing of APP and a neurotoxic "Aβ cascade". As such, altered signaling from PTPσ after traumatic brain injury and ischemic stroke may explain how these risk factors can trigger subsequent onset of AD. Restoring the integrity of brain microenvironment therefore could be essential in preventing AD for the population at risk.

References:

1. **Selkoe, D.J. Alzheimer's disease. *Cold Spring Harbor perspectives in biology* 3(2011).**
2. **Yan, R. & Vassar, R. Targeting the beta secretase BACE1 for Alzheimer's disease therapy. *The Lancet. Neurology* 13, 319-329 (2014).**
3. **Mikulca, J.A., *et al.* Potential novel targets for Alzheimer pharmacotherapy: II. Update on secretase inhibitors and related approaches. *Journal of clinical pharmacy and therapeutics* 39, 25-37 (2014).**
4. **De Strooper, B. Lessons from a failed gamma-secretase Alzheimer trial. *Cell* 159, 721-726 (2014).**
5. **Arriagada, P.V., Growdon, J.H., Hedley-Whyte, E.T. & Hyman, B.T. Neurofibrillary tangles but not senile plaques parallel duration and severity of Alzheimer's disease. *Neurology* 42, 631-639 (1992).**
6. **Bouras, C., Hof, P.R., Giannakopoulos, P., Michel, J.P. & Morrison, J.H. Regional distribution of neurofibrillary tangles and senile plaques in the cerebral cortex of elderly patients: a quantitative evaluation of a one-year autopsy population from a geriatric hospital. *Cerebral cortex* 4, 138-150 (1994).**
7. **Wang, Y. & Mandelkow, E. Tau in physiology and pathology. *Nature reviews. Neuroscience* 17, 5-21 (2016).**
8. **Aricescu, A.R., McKinnell, I.W., Halfter, W. & Stoker, A.W. Heparan sulfate proteoglycans are ligands for receptor protein tyrosine phosphatase sigma. *Molecular and cellular biology* 22, 1881-1892 (2002).**
9. **Shen, Y., *et al.* PTPsigma is a receptor for chondroitin sulfate proteoglycan, an inhibitor of neural regeneration. *Science* 326, 592-596 (2009).**
10. **Coles, C.H., *et al.* Proteoglycan-specific molecular switch for RPTPsigma clustering and neuronal extension. *Science* 332, 484-488 (2011).**
11. **Wang, H., *et al.* Expression of receptor protein tyrosine phosphatase-sigma (RPTP-sigma) in the nervous system of the developing and adult rat. *Journal of neuroscience research* 41, 297-310 (1995).**
12. **Yan, H., *et al.* A novel receptor tyrosine phosphatase-sigma that is highly expressed in the nervous system. *The Journal of biological chemistry* 268, 24880-24886 (1993).**
13. **Chow, V.W., Mattson, M.P., Wong, P.C. & Gleichmann, M. An overview of APP processing enzymes and products. *Neuromolecular medicine* 12, 1-12 (2010).**
14. **Nunan, J. & Small, D.H. Regulation of APP cleavage by alpha-, beta- and gamma-secretases. *FEBS letters* 483, 6-10 (2000).**
15. **Estus, S., *et al.* Potentially amyloidogenic, carboxyl-terminal derivatives of the amyloid protein precursor. *Science* 255, 726-728 (1992).**
16. **Davis, J., *et al.* Early-onset and robust cerebral microvascular accumulation of amyloid beta-protein in transgenic mice expressing low levels of a vasculotropic Dutch/Iowa mutant form of amyloid beta-protein precursor. *The Journal of biological chemistry* 279, 20296-20306 (2004).**

17. Mucke, L., *et al.* High-level neuronal expression of abeta 1-42 in wild-type human amyloid protein precursor transgenic mice: synaptotoxicity without plaque formation. *The Journal of neuroscience : the official journal of the Society for Neuroscience* 20, 4050-4058 (2000).
18. Fleck, D., Garratt, A.N., Haass, C. & Willem, M. BACE1 dependent neuregulin processing: review. *Current Alzheimer research* 9, 178-183 (2012).
19. Luo, X., *et al.* Cleavage of neuregulin-1 by BACE1 or ADAM10 protein produces differential effects on myelination. *The Journal of biological chemistry* 286, 23967-23974 (2011).
20. Cheret, C., *et al.* Bace1 and Neuregulin-1 cooperate to control formation and maintenance of muscle spindles. *The EMBO journal* 32, 2015-2028 (2013).
21. De Strooper, B., *et al.* A presenilin-1-dependent gamma-secretase-like protease mediates release of Notch intracellular domain. *Nature* 398, 518-522 (1999).
22. Tian, Y., Bassit, B., Chau, D. & Li, Y.M. An APP inhibitory domain containing the Flemish mutation residue modulates gamma-secretase activity for Abeta production. *Nature structural & molecular biology* 17, 151-158 (2010).
23. Zhang, Z., *et al.* Presenilins are required for gamma-secretase cleavage of beta-APP and transmembrane cleavage of Notch-1. *Nature cell biology* 2, 463-465 (2000).
24. Glass, C.K., Saijo, K., Winner, B., Marchetto, M.C. & Gage, F.H. Mechanisms underlying inflammation in neurodegeneration. *Cell* 140, 918-934 (2010).
25. DeWitt, D.A., Perry, G., Cohen, M., Doller, C. & Silver, J. Astrocytes regulate microglial phagocytosis of senile plaque cores of Alzheimer's disease. *Experimental neurology* 149, 329-340 (1998).
26. Frederickson, R.C. Astroglia in Alzheimer's disease. *Neurobiology of aging* 13, 239-253 (1992).
27. Horn, K.E., *et al.* Receptor protein tyrosine phosphatase sigma regulates synapse structure, function and plasticity. *Journal of neurochemistry* 122, 147-161 (2012).
28. Tomidokoro, Y., *et al.* Abeta amyloidosis induces the initial stage of tau accumulation in APP(Sw) mice. *Neuroscience letters* 299, 169-172 (2001).
29. Sturchler-Pierrat, C., *et al.* Two amyloid precursor protein transgenic mouse models with Alzheimer disease-like pathology. *Proceedings of the National Academy of Sciences of the United States of America* 94, 13287-13292 (1997).
30. Rockenstein, E., Mallory, M., Mante, M., Sisk, A. & Masliaha, E. Early formation of mature amyloid-beta protein deposits in a mutant APP transgenic model depends on levels of Abeta(1-42). *Journal of neuroscience research* 66, 573-582 (2001).
31. Holtzman, D.M., *et al.* Tau: From research to clinical development. *Alzheimer's & dementia : the journal of the Alzheimer's Association* (2016).
32. Morris, M., *et al.* Tau post-translational modifications in wild-type and human amyloid precursor protein transgenic mice. *Nature neuroscience* 18, 1183-1189 (2015).

33. **Daffner, K.R.*, et al.* Pathophysiology underlying diminished attention to novel events in patients with early AD. *Neurology* 56, 1377-1383 (2001).**
34. **Daffner, K.R., Mesulam, M.M., Cohen, L.G. & Scinto, L.F. Mechanisms underlying diminished novelty-seeking behavior in patients with probable Alzheimer's disease. *Neuropsychiatry, neuropsychology, and behavioral neurology* 12, 58-66 (1999).**
35. **Marin, R.S., Biedrzycki, R.C. & Firinciogullari, S. Reliability and validity of the Apathy Evaluation Scale. *Psychiatry research* 38, 143-162 (1991).**
36. **Kaufman, D.A., Bowers, D., Okun, M.S., Van Patten, R. & Perlstein, W.M. Apathy, Novelty Processing, and the P3 Potential in Parkinson's Disease. *Frontiers in neurology* 7, 95 (2016).**
37. **Johnson, V.E., Stewart, W. & Smith, D.H. Traumatic brain injury and amyloid-beta pathology: a link to Alzheimer's disease? *Nature reviews. Neuroscience* 11, 361-370 (2010).**
38. **Sivanandam, T.M. & Thakur, M.K. Traumatic brain injury: a risk factor for Alzheimer's disease. *Neuroscience and biobehavioral reviews* 36, 1376-1381 (2012).**
39. **Kalaria, R.N. The role of cerebral ischemia in Alzheimer's disease. *Neurobiology of aging* 21, 321-330 (2000).**
40. **Cole, S.L. & Vassar, R. Linking vascular disorders and Alzheimer's disease: potential involvement of BACE1. *Neurobiology of aging* 30, 1535-1544 (2009).**
41. **Emmerling, M.R.*, et al.* Traumatic brain injury elevates the Alzheimer's amyloid peptide A beta 42 in human CSF. A possible role for nerve cell injury. *Annals of the New York Academy of Sciences* 903, 118-122 (2000).**
42. **Olsson, A.*, et al.* Marked increase of beta-amyloid(1-42) and amyloid precursor protein in ventricular cerebrospinal fluid after severe traumatic brain injury. *Journal of neurology* 251, 870-876 (2004).**
43. **Loane, D.J.*, et al.* Amyloid precursor protein secretases as therapeutic targets for traumatic brain injury. *Nature medicine* 15, 377-379 (2009).**
44. **Pluta, R., Furmaga-Jablonska, W., Maciejewski, R., Ulamek-Koziol, M. & Jablonski, M. Brain ischemia activates beta- and gamma-secretase cleavage of amyloid precursor protein: significance in sporadic Alzheimer's disease. *Molecular neurobiology* 47, 425-434 (2013).**
45. **Washington, P.M.*, et al.* The effect of injury severity on behavior: a phenotypic study of cognitive and emotional deficits after mild, moderate, and severe controlled cortical impact injury in mice. *Journal of neurotrauma* 29, 2283-2296 (2012).**
46. **Kokiko-Cochran, O.*, et al.* Altered Neuroinflammation and Behavior after Traumatic Brain Injury in a Mouse Model of Alzheimer's Disease. *Journal of neurotrauma* (2015).**
47. **Tajiri, N., Kellogg, S.L., Shimizu, T., Arendash, G.W. & Borlongan, C.V. Traumatic brain injury precipitates cognitive impairment and extracellular Abeta aggregation in Alzheimer's disease transgenic mice. *PloS one* 8, e78851 (2013).**
48. **Watanabe, T., Takasaki, K., Yamagata, N., Fujiwara, M. & Iwasaki, K. Facilitation of memory impairment and cholinergic disturbance in a mouse**

model of Alzheimer's disease by mild ischemic burden. *Neuroscience letters* 536, 74-79 (2013).

49. Properzi, F., *et al.* Chondroitin 6-sulphate synthesis is up-regulated in injured CNS, induced by injury-related cytokines and enhanced in axon-growth inhibitory glia. *The European journal of neuroscience* 21, 378-390 (2005).

50. Yi, J.H., *et al.* Alterations in sulfated chondroitin glycosaminoglycans following controlled cortical impact injury in mice. *The Journal of comparative neurology* 520, 3295-3313 (2012).

51. Hill, J.J., Jin, K., Mao, X.O., Xie, L. & Greenberg, D.A. Intracerebral chondroitinase ABC and heparan sulfate proteoglycan glypican improve outcome from chronic stroke in rats. *Proceedings of the National Academy of Sciences of the United States of America* 109, 9155-9160 (2012).

52. Huang, L., *et al.* Glial scar formation occurs in the human brain after ischemic stroke. *International journal of medical sciences* 11, 344-348 (2014).

53. Celio, M.R. & Blumcke, I. Perineuronal nets--a specialized form of extracellular matrix in the adult nervous system. *Brain research. Brain research reviews* 19, 128-145 (1994).

54. Cregg, J.M., *et al.* Functional regeneration beyond the glial scar. *Experimental neurology* 253, 197-207 (2014).

55. Soleman, S., Filippov, M.A., Dityatev, A. & Fawcett, J.W. Targeting the neural extracellular matrix in neurological disorders. *Neuroscience* 253, 194-213 (2013).

56. DeWitt, D.A., Silver, J., Canning, D.R. & Perry, G. Chondroitin sulfate proteoglycans are associated with the lesions of Alzheimer's disease. *Experimental neurology* 121, 149-152 (1993).

57. Patey, S.J., Edwards, E.A., Yates, E.A. & Turnbull, J.E. Heparin derivatives as inhibitors of BACE-1, the Alzheimer's beta-secretase, with reduced activity against factor Xa and other proteases. *Journal of medicinal chemistry* 49, 6129-6132 (2006).

58. Li, J., *et al.* Expression of heparanase in vascular cells and astrocytes of the mouse brain after focal cerebral ischemia. *Brain research* 1433, 137-144 (2012).

59. Elchebly, M., *et al.* Neuroendocrine dysplasia in mice lacking protein tyrosine phosphatase sigma. *Nature genetics* 21, 330-333 (1999).

Supplementary Materials:

Materials and Methods:

Mouse lines: Mice were maintained under standard conditions approved by the Institutional Animal Care and Use Committee. Wild type and PTPσ-deficient mice of Balb/c background were provided by Dr. Michel L. Tremblay [59]. Homozygous TgAPP-SwDI mice, C57BL/6-Tg(Thy1-APPSwDutIowa)BWevn/Mmjax, stock number 007027, were from the Jackson Laboratory. These mice express human APP transgene harboring Swedish, Dutch, and Iowa mutations, and were bred with Balb/c mice heterozygous for the PTPσ gene to generate bigenic mice heterozygous for both TgAPP-SwDI and PTPσ genes, which are hybrids of 50% C57BL/6J and 50% Balb/c genetic background. These mice were further bred with Balb/c mice heterozygous for the PTPσ gene. The offspring from this mating are used in experiments, which include littermates of the following genotypes: TgAPP-SwDI(+/-)PTPσ(+/+), mice heterozygous for TgAPP-SwDI transgene with wild type PTPσ; TgAPP-SwDI(+/-)PTPσ(-/-), mice heterozygous for TgAPP-SwDI transgene with genetic depletion of PTPσ; TgAPP-SwDI(-/-)PTPσ(+/+), mice free of TgAPP-SwDI transgene with wild type PTPσ. Both TgAPP-SwDI(-/-)PTPσ(+/+) and Balb/c PTPσ(+/+) are wild type mice but with different genetic background. Heterozygous TgAPP-SwInd (J20) mice, 6.Cg-Tg(PDGFB-APPSwInd)20Lms/2Mmjax, were provided by Dr. Lennart Mucke. These mice express human APP transgene harboring Swedish and Indiana mutations, and were bred with the same strategy as described above to obtain mice with genotypes of TgAPP-SwInd (+/-)PTPσ(+/+) and TgAPP-SwInd (+/-)PTPσ(-/-).

Antibodies:

Primary Antibodies	Application	Clone #	Catalog #	Supplier
Mouse anti-Actin	WB	AC-40	A4700	Sigma-Aldrich
Rabbit anti-APH1	WB		PA5-20318	Thermo Scientific
Rabbit anti-APP C-term	WB, IP, IHC	Y188	NB110-55461	Novus Biologicals
Mouse anti-murine Aβ, 1-16	WB, IP	M3.2	805701	Biolegend
Mouse anti-human Aβ, 1-16	WB, IP, IHC, ELISA	6E10	803001	Biolegend
Mosue anti-Aβ, 17-24	WB, IHC	4G8	SIG-39220	Biolegend
Mouse HRP-conjugated anti-Aβ 1-40	ELISA	11A50-B10	SIG-39146	Biolegend
Mouse HRP-conjugated anti-Aβ 1-42	ELISA	12F4	805507	Biolegend
Rabbit anti-BACE1 C-Term, B690	WB		PRB-617C	Covance
Guinea Pig anti-BACE1 C-Term	IP		840201	Biolegend
Chiken anti-GFAP	IHC		ab4674	Abcam
Rabbit anti-Neuregulin	WB		sc-348	Santa Cruz Biotechnology
Rabbit anti-Nicastrin	WB		5665	Cell Signaling
Rabbit anti-Notch NICD (val1744)	WB		4147	Cell Signaling
Rabbit anti-Notch (C-20)	WB		sc-6014R	Santa Cruz Biotechnology
Rabbit anti-PEN2	WB		8598	Cell Signaling
Rabbit anti-Presenilin 1/2 NTF	WB		840201	Abcam
Rabbit anti-Presenilin 1 CTF	WB		5643	Cell Signaling
Rabbit anti-Presenilin 2 CTF	WB		9979	Cell Signaling
Mouse anti-PTPσ ICD	WB, IHC	17G7.2	MM-002-P	Medimabs
Mouse anti-PTPσ ECD	WB		ab55640	Abcam
Rabbit anti-Synaptophysin	IHC		AB9272	Millipore
Mouse anti-Tau	WB, IHC	Tau-5	MAB361	Millipore
Mouse anti-Tau	IHC	Tau-46	4019	Cell Signaling
Secondary and Tertiary Antibodies	**Application**	**Clone #**	**Catalog #**	**Supplier**
Goat anti-mouse IgG HRP-conjugated	WB		7076S	Cell Signaling
Goat anti-rabbit IgG HRP-conjugated	WB		7074S	Cell Signaling
Goat anti-mouse IgG Alexa488	IHC		A-11001	Invitrogen
Donkey anti-goat IgG Alexa488	IHC		A-11055	Invitrogen
Chicken anti-rabbit IgG CF568	IHC		SAB4600426	Sigma-Aldrich
Donkey anti-chicken IgG Cy3	IHC		703-165-155	JacksonImmunoResearch

Immunohistochemistry: Adult rat and mice were perfused intracardially with fresh made 4% paraformaldehyde in cold phosphate-buffered saline (PBS). The brains were collected and post-fixed for 2 days at 4 °C. Paraffin embedded sections of 10 μM thickness were collected for immunostaining. The sections were deparaffinized and sequentially rehydrated. Antigen retrieval was performed at 100 °C in Tris-EDTA buffer (pH 9.0) for 50 min. Sections were subsequently washed with distilled water and PBS, incubated at room temperature for 1 hour in blocking buffer (PBS, with 5% normal donkey serum, 5% normal goat serum, and 0.2% Triton X-100). Primary antibody

incubation was performed in a humidified chamber at 4°C overnight. After 3 washes in PBS with 0.2% Triton X-100, the sections were then incubated with a mixture of secondary and tertiary antibodies at room temperature for 2 hours. All antibodies were diluted in blocking buffer with concentrations recommended by the manufacturers. Mouse primary antibodies were detected by goat anti-mouse Alexa488 together with donkey anti-goat Alexa488 antibodies; rabbit primary antibodies were detected by chicken anti-rabbit CF568 and donkey anti-chicken Cy3 antibodies; chicken antibody was detected with donkey anti-chicken Cy3 antibody. Sections stained with only secondary and tertiary antibodies (without primary antibodies) were used as negative controls. At last, DAPI (Invitrogen, 300 nM) was applied on sections for nuclear staining. Sections were washed 5 times before mounted in Fluoromount (SouthernBiotech).

Wide field and confocal images were captured using Zeiss Axio Imager M2 and LSM780, respectively. Images are quantified using the Zen 2 Pro software and ImageJ.

Protein extraction, immunoprecipitation, and western blot analysis: For the co-immunoprecipitation of APP and PTPσ, RIPA buffer was used (50 mM Tris-HCl, pH 8.0, 1 mM EDTA, 150 mM NaCl, 1% NP40, 0.1% SDS, 0.5% sodium deoxycholate). For the co-immunoprecipitation of APP and BACE1, NP40 buffer was used (50 mM Tris-HCl, pH 8.0, 1 mM EDTA, 150 mM NaCl, 1% NP40) without or with SDS at concentration of 0.1%, 0.3%, and 0.4%. For total protein extraction and immunopurification of CTFβ, SDS concentration in RIPA buffer was adjusted to 1% to ensure protein extraction from the lipid rafts. Mouse or rat forebrains were homogenized thoroughly on ice in homogenization buffers (as mention above) containing protease and

phosphatase inhibitors (Thermo Scientific). For each half of forebrain, buffer volume of at least 5 ml for mouse and 8 ml for rat was used to ensure sufficient detergent/tissue ratio. The homogenates were incubated at 4°C for 1 hour with gentle mixing, sonicated on ice for 2 minutes in a sonic dismembrator (Fisher Scientific Model 120, with pulses of 50% output, 1 second on and 1 second off), followed with another hour of gentle mixing at 4°C. All samples were used fresh without freezing and thawing.

For co-immunoprecipitation and immunopurification, the homogenates were then centrifuged at 85,000 x g for 1 hour at 4°C and the supernatants were collected. Protein concentration was measured using BCA Protein Assay Kit (Thermo Scientific). 0.5 mg total proteins of brain homogenates were incubated with 5 μg of designated antibody and 30 μl of Protein-A sepharose beads (50% slurry, Roche), in a total volume of 1 ml adjusted with RIPA buffer. Samples were gently mixed at 4°C overnight. Subsequently, the beads were washed 5 times with cold immunoprecipitation buffer. Samples were then incubated in Laemmli buffer with 100 mM of DTT at 75°C for 20 minutes and subjected to western blot analysis.

For analysis of protein expression level, the homogenates were centrifuged at 23,000 x g for 30 min at 4°C and the supernatants were collected. Protein concentration was measured using BCA Protein Assay Kit (Thermo Scientific). 30 μg of total proteins were subjected to western blot analysis.

Electrophoresis of protein samples was conducted using 4-12% Bis-Tris Bolt Plus Gels, with either MOPS or MES buffer and Novex Sharp Pre-stained Protein Standard (all from Invitrogen). Proteins were transferred to nitrocellulose membrane (0.2 μm pore size, Bio-Rad) and blotted with selected antibodies (see table above) at concentrations

suggested by the manufacturers. Primary antibodies were diluted in SuperBlock TBS Blocking Buffer (Thermo Scientific) and incubated with the nitrocellulose membranes at 4°C overnight; secondary antibodies were diluted in PBS with 5% nonfat milk and 0.2% Tween20 and incubated at room temperature for 2 hours. Membranes were washes 4 times in PBS with 0.2% Tween20 between primary and secondary antibodies and before chemiluminescent detection with SuperSignal West Pico Chemiluminescent Substrate (Thermo Scientific).

Western blot band intensity was quantified by densitometry.

Aβ ELISA assays: Mouse forebrains were thoroughly homogenized in tissue homogenization buffer (2 mM Tris pH 7.4, 250 mM sucrose, 0.5 mM EDTA, 0.5 mM EGTA) containing protease inhibitor cocktail (Roche), followed by centrifugation at 135,000 x g (33,500 RPM with SW50.1 rotor) for 1 hour at 4°C. Proteins in the pellets were extracted with formic acid (FA) and centrifuged at 109,000 x g (30,100 RPM with SW50.1 rotor) for 1 hour at 4°C. The supernatants were collected and diluted 1:20 in neutralization buffer (1 M Tris base, 0.5 M Na_2HPO_4, 0.05% NaN_3) and subsequently 1:3 in ELISA buffer (PBS with 0.05% Tween-20, 1% BSA, and 1 mM AEBSF). Diluted samples were loaded onto ELISA plates pre-coated with 6E10 antibody (Biolegend) to capture Aβ peptides. Serial dilutions of synthesized human Aβ 1-40 or 1-42 (American Peptide) were loaded to determine a standard curve. Aβ was detected using an HRP labeled antibody for either Aβ 1-40 or 1-42 (see table above). ELISA was developed using TMB substrate (Thermo Scientific) and reaction was stopped with 1N HCl. Plates

were read at 450nm and concentrations of Aβ in samples were determined using the standard curve.

Behavior assays: The Y-maze assay: Mice were placed in the center of the Y-maze and allowed to move freely through each arm. Their exploratory activities were recorded for 5 minutes. An arm entry is defined as when all four limbs are within the arm. For each mouse, the number of triads is counted as "spontaneous alternation", which was then divided by the number of total arm entries, yielding a percentage score. The novel object test: On day 1, mice were exposed to empty cages (45 cm x 24 cm x 22 cm) with blackened walls to allow exploration and habituation to the arena. During day 2 to day 4, mice were returned to the same cage with two identical objects placed at an equal distance. On each day mice were returned to the cage at approximately the same time during the day and allowed to explore for 10 minutes. Cages and objects were cleaned with 70% ethanol between each animal. Subsequently, 2 hours after the familiarization session on day 4, mice were put back to the same cage where one of the familiar objects (randomly chosen) was replaced with a novel object, and allowed to explore for 5 minutes. Mice were scored using Observer software (Noldus) on their time duration and visiting frequency exploring either object. Object exploration was defined as facing the object and actively sniffing or touching the object, whereas any climbing behavior was not scored. The discrimination indexes reflecting interest in the novel object is denoted as either the ratio of novel object exploration to total object exploration (NO/NO+FO) or the ratio of novel object exploration to familiar object exploration (NO/FO). All tests and data analyses were conducted in a double-blinded manner.

Statistics: 2-tailed Student's *t* test was used for two-group comparison. Relationship between two variables (SDS concentration and APP-BACE1 association, as in Fig 3) was analyzed using linear regression. All error bars show standard error of the means (SEM).

Figure 1. PTPσ is an APP binding partner in the brain.

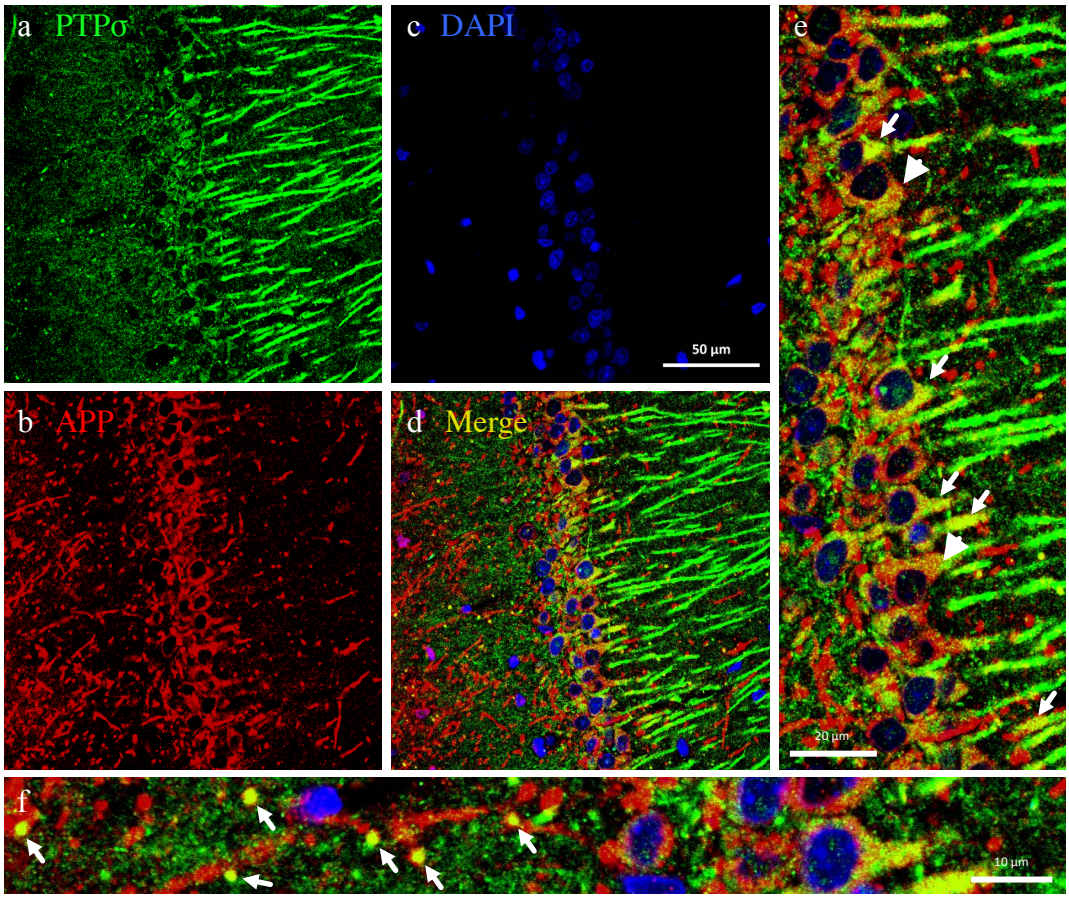

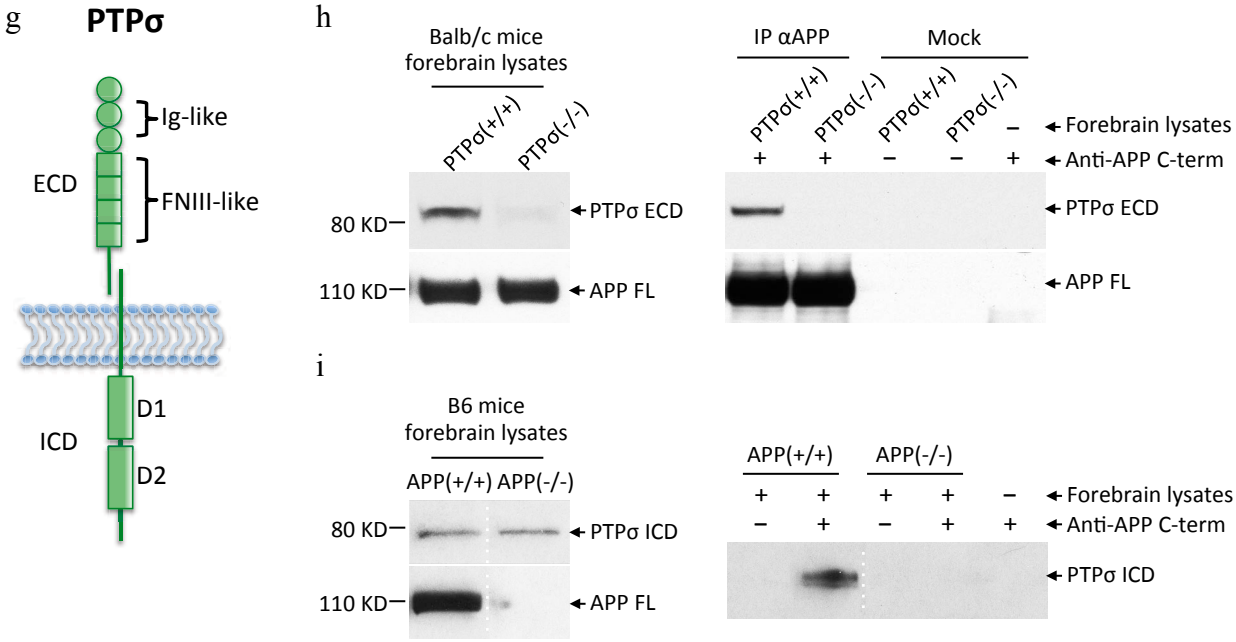

Figure 1. PTPσ is an APP binding partner in the brain. a-f, Colocalization of PTPσ (**a**, green) and APP (**b,** red) in hippocampal CA1 neurons of adult rat is shown by confocal imaging. Nuclei of CA1 neurons are stained with DAPI (**c**, blue). **d**, Merge of three channels. Scale bar, 50 μm. **e**, Zoom-in image of the soma layer in **d**. Arrows, intensive colocalization of PTPσ and APP in the initial segments of apical dendrites; arrow heads, punctates of colocalization in the perinuclear regions. Scale bar, 20 μm. **f**, Zoom-in image of the very fine grained punctates in the axonal compartment in **d**. Arrows points to the colocalization of PTPσ and APP in axons projecting perpendicular to the focal plane. Scale bar, 10 μm. **g**, Schematic diagram of PTPσ expressed on cell surface as a two-subunit complex. PTPσ is post-translationally processed into an extracellular domain (ECD) and a transmembrane-intracellular domain (ICD). These two subunits associate with each other through noncovalent bond. Ig-like, immunoglobulin-like domains; FNIII-like, fibronectin III-like domains; D1 and D2, two phosphatase domains. **h**, **i**, Co-immunoprecipitation (co-IP) of PTPσ and APP from mouse forebrain lysates. Left panels, expression of PTPσ and APP in mouse forebrains. Right panels, IP using an antibody specific for the C-terminus (C-term) of APP. Full length APP (APP FL) is detected by anti-APP C-term antibody. **h**, PTPσ co-IP with APP from forebrain lysates of wild type but not PTPσ-deficient mice (Balb/c background), detected by an antibody against PTPσ-ECD. **i**, PTPσ co-IP with APP from forebrain lysates of wild type but not APP knockout mice (B6 background), detected by an antibody against PTPσ-ICD. Dotted lines in **i** indicate lanes on the same western blot exposure that were moved adjacent to each other. Images shown are representatives of at least three independent experiments.

Extended Data Figure 1. Molecular complex of PTPσ and APP in brains of various rodent species.

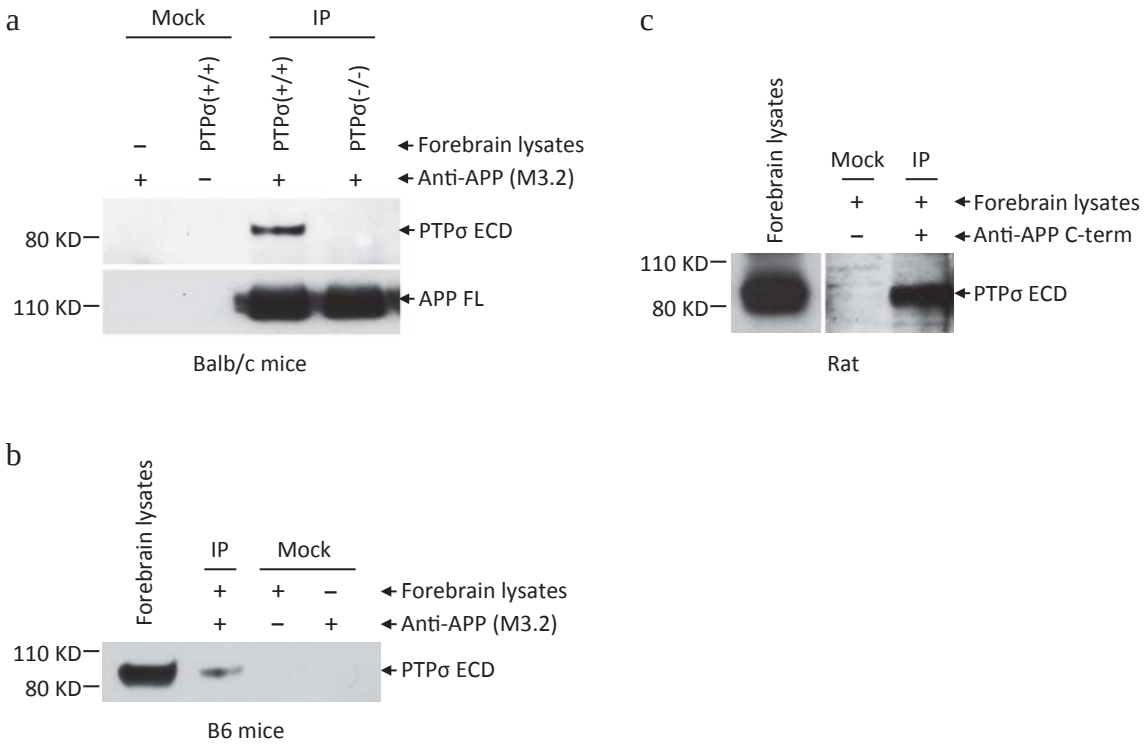

Extended Data Figure 1. Molecular complex of PTPσ and APP in brains of various rodent species. a, **b**, Co-immunoprecipitation using an anti-APP antibody specific for amino acid residues 1-16 of mouse Aβ (clone M3.2). PTPσ and APP binding interaction is detected in forebrains of Balb/c (**a**) and B6 (**b**) mice. **c**, PTPσ co-immunoprecipitates with APP from rat forebrain lysates using an antibody specific for the C-terminus of APP. Images shown are representatives of at least three independent experiments.

Figure 2. Genetic depletion of PTPσ reduces β-amyloidogenic products of APP.

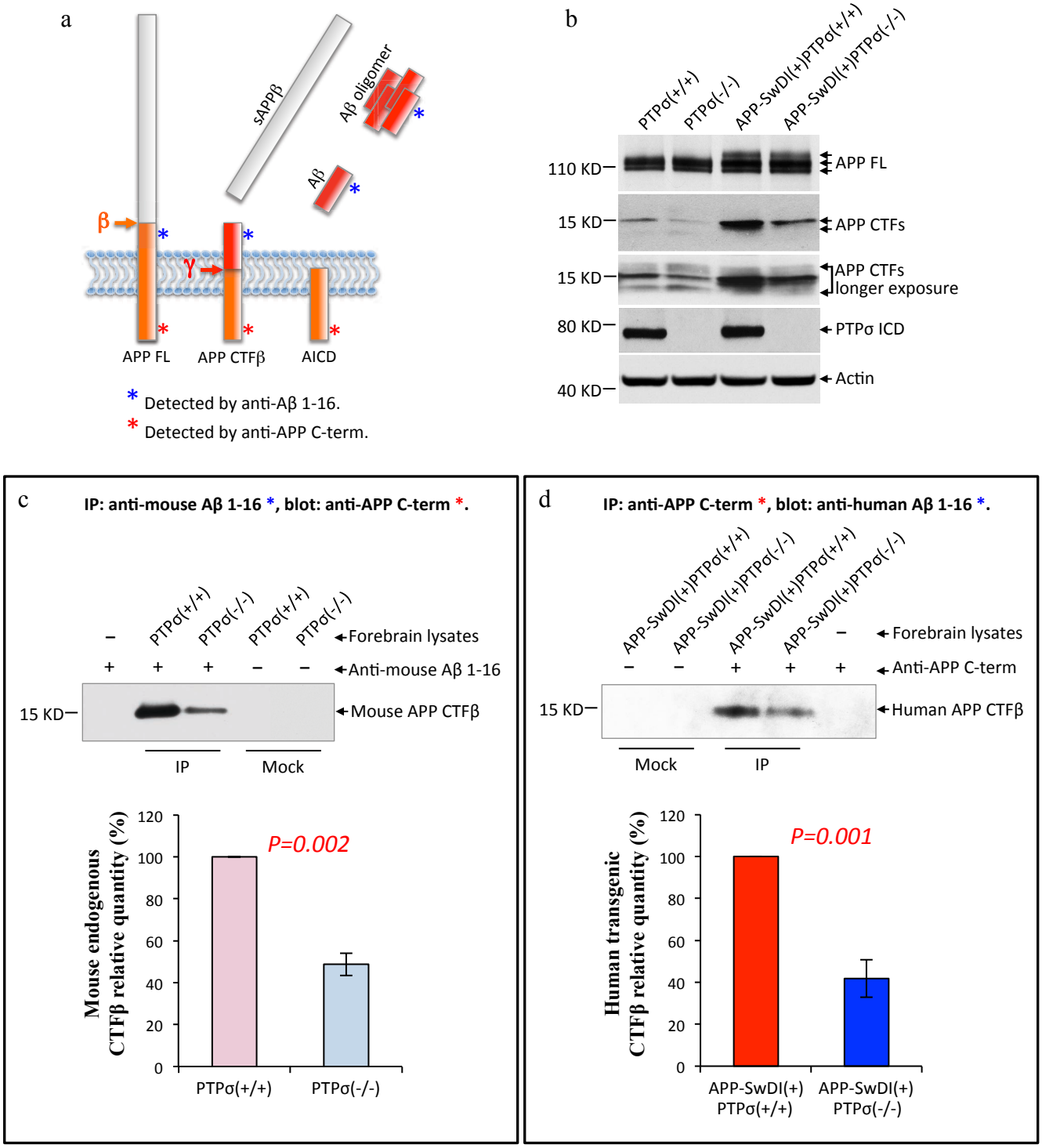

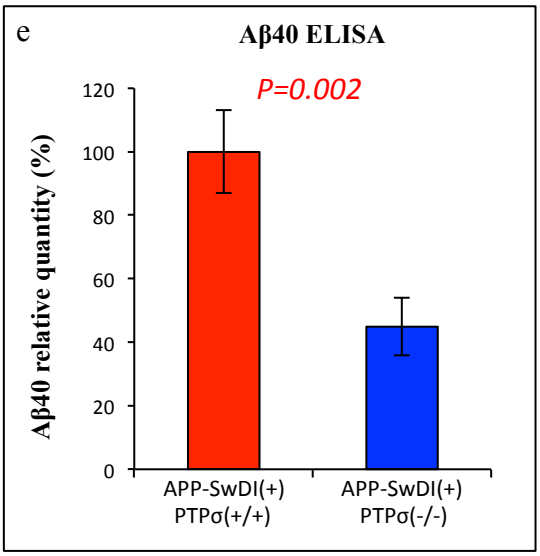
e
Aβ40 ELISA
P=0.002
Aβ40 relative quantity (%)
120
100
80
60
40
20
0
APP-SwDI(+) PTPσ(+/+)
APP-SwDI(+) PTPσ(-/-)

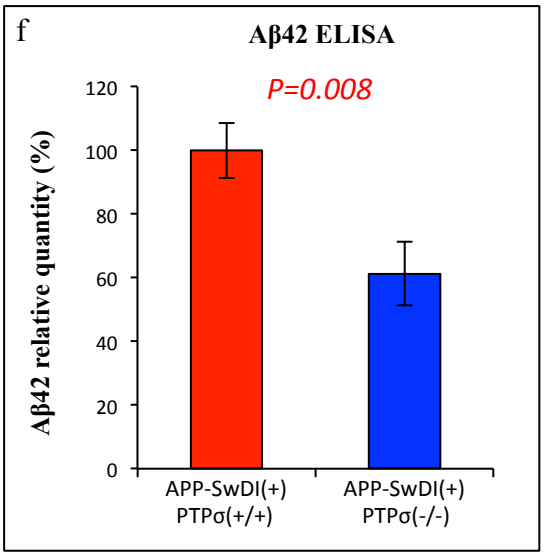
f
Aβ42 ELISA
P=0.008
Aβ42 relative quantity (%)
120
100
80
60
40
20
0
APP-SwDI(+) PTPσ(+/+)
APP-SwDI(+) PTPσ(-/-)

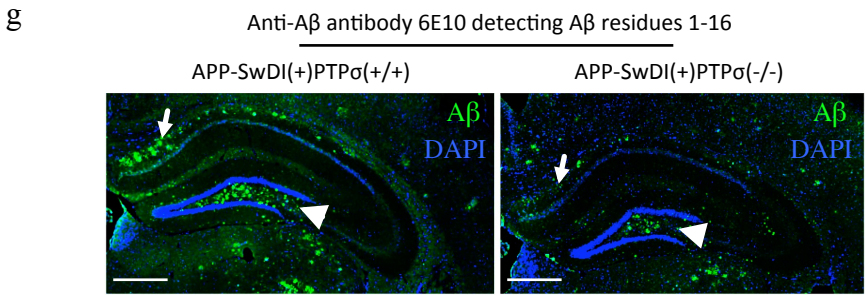
g
Anti-Aβ antibody 6E10 detecting Aβ residues 1-16
APP-SwDI(+)PTPσ(+/+)
APP-SwDI(+)PTPσ(-/-)
Aβ
DAPI
Aβ
DAPI

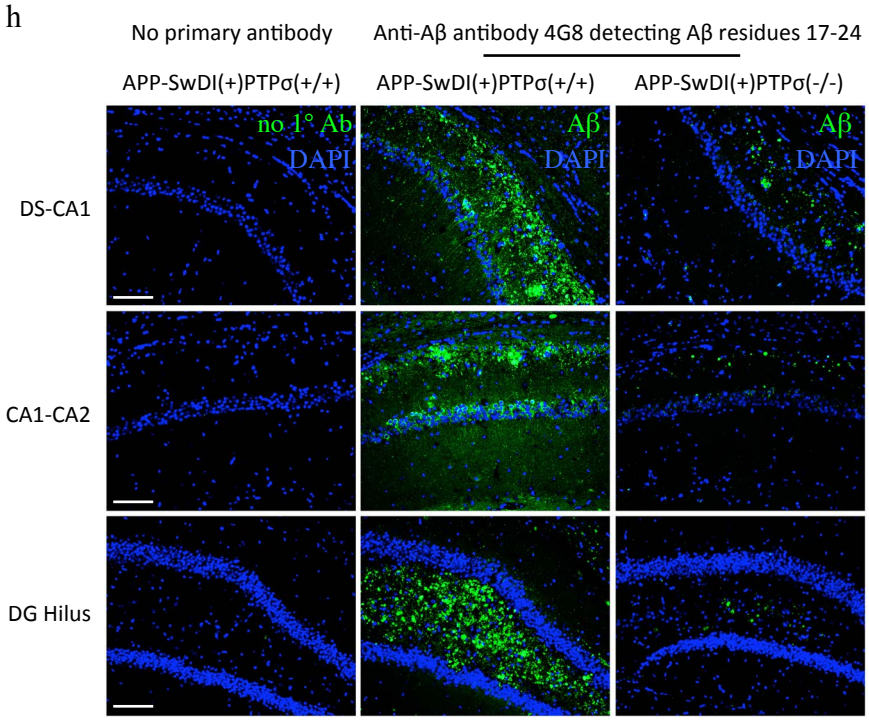
h
No primary antibody
Anti-Aβ antibody 4G8 detecting Aβ residues 17-24
APP-SwDI(+)PTPσ(+/+)
APP-SwDI(+)PTPσ(+/+)
APP-SwDI(+)PTPσ(-/-)
no 1° Ab
DAPI
Aβ
DAPI
Aβ
DAPI
DS-CA1
CA1-CA2
DG Hilus

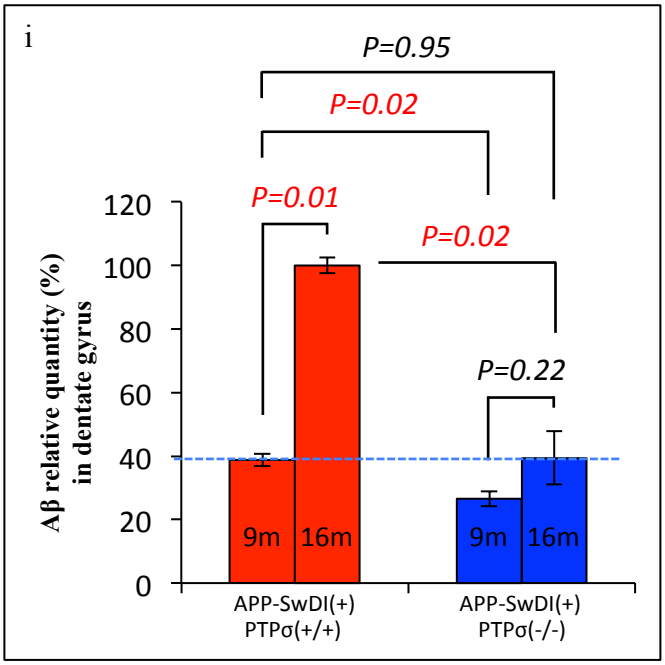
i
P=0.95
P=0.02
P=0.01
P=0.02
P=0.22
Aβ relative quantity (%)
in dentate gyrus
120
100
80
60
40
20
0
9m
16m
9m
16m
APP-SwDI(+)
PTPσ(+/+)
APP-SwDI(+)
PTPσ(-/-)

Figure 2. Genetic depletion of PTPσ reduces β-amyloidogenic products of APP. a, Schematic diagram showing amyloidogenic processing of APP by the β- and γ-secretases. Full length APP (APP FL) is cleaved by β-secretase into soluble N-terminal (sAPPβ) and C-terminal (CTFβ) fragments. APP CTFβ can be further processed by γ-secretase into a C-terminal intracellular domain (AICD) and an Aβ peptide. Aggregation of Aβ is a definitive pathology hallmark of AD. **b**, PTPσ deficiency reduces the level of an APP CTF at about 15 KD in mouse forebrain lysates, without affecting the expression of APP FL. Antibody against the C-terminus of APP recognizes APP FL and CTFs of both mouse and human origins. **c** and **d**, The 15 KD APP CTF is identified as CTFβ by immunoprecipitation (IP) followed with western blot analysis, using a pair of antibodies as marked in the diagram (**a**). Antibodies against amino acids 1-16 of Aβ (anti-Aβ 1-16) detect CTFβ but not CTFα, as the epitope is absent in CTFα. **c**, Mouse endogenous CTFβ level is reduced in PTPσ-deficient mouse brains. 4 repeated experiments were quantified by densitometry. **d**, Human transgenic CTFβ level is reduced in PTPσ-deficient mouse brains harboring human APP-SwDI transgene. 6 repeated experiments were quantified by densitometry. Within each experiment in both **c** and **d**, the value from PTPσ deficient sample was normalized to that from the sample with wild type PTPσ. **e** and **f**, PTPσ deficiency reduces the levels of Aβ40 (**e**) and Aβ42 (**f**) in TgAPP-SwDI mice as measured by ELISA assays. n=12 for each group. The mean values from PTPσ deficient samples was normalized to that from the samples with wild type PTPσ. **g** and **h**, Aβ deposition in the hippocampus of 10-month old TgAPP-SwDI mice. Aβ (green) is detected by immunofluorescent staining using anti-Aβ antibodies clone 6E10 (**g**) and clone 4G8 (**h**). DAPI staining is shown in blue. PTPσ deficiency significantly decreases Aβ burden in the brains of TgAPP-SwDI mice. **h**, Upper panels, the stratum oriens layer between dorsal subiculum (DS) and CA1 (also shown with arrows in **g**); middle panels, oriens layer between CA1 and CA2; lower panels, the hilus of dentate gyrus (DG, also shown with arrow heads in **g**). Left column, control staining without primary antibody (no 1° Ab). No Aβ signal is detected in non-transgenic mice (data not shown). Scale bars, 500 μm in **G** and 100 μm in **h**. Images shown are a representative pair among 5 pairs of age- and sex-matched mice of 9- to 11-month old. **i**, Genetic depletion of PTPσ suppresses the progression of Aβ pathology in TgAPP-SwDI mice. ImageJ quantification of Aβ immunofluorescent staining (with 6E10) in DG hilus from 9- and 16-month old TgAPP-SwDI mice. n=3 for each group. Total integrated density of Aβ in DG hilus was normalized to the area size of the hilus to yield the average intensity as show in the bar graph. Mean value of each group was normalized to that of 16 month old TgAPP-SwDI mice expressing wild type PTPσ. All *p* values, Student's *t* test, 2-tailed. Error bars, SEM.

Extended Data Figure 2. Genetic depletion of PTPσ reduces β-amyloidogenic products of APP.

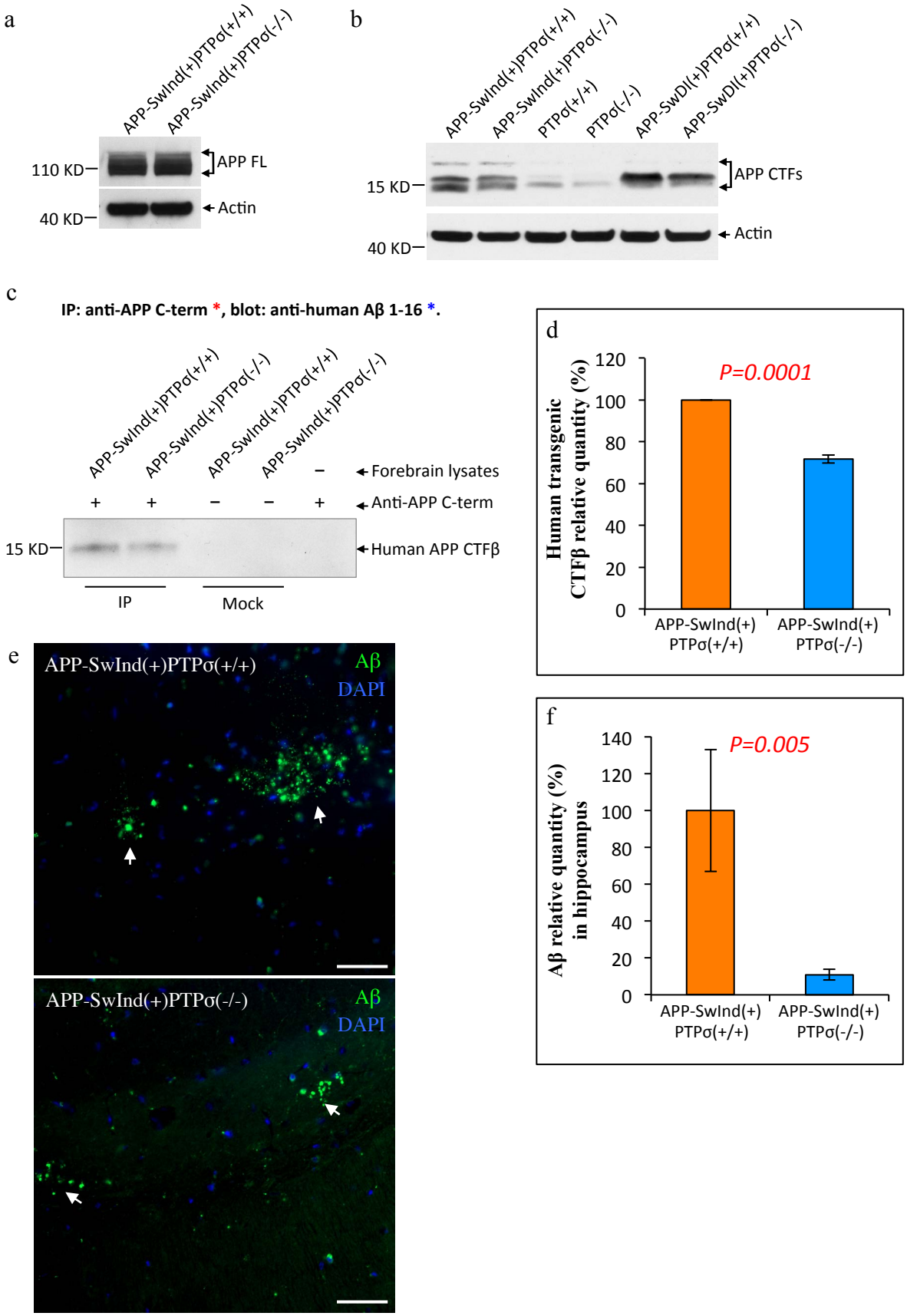

Extended Data Figure 2. Genetic depletion of PTPσ reduces β-amyloidogenic products of APP. a and **b**, Antibody against the C-terminus of APP recognizes full length (FL) and C-terminal fragments (CTFs) of both mouse and human APP. PTPσ deficiency does not affect the expression level of APP FL (**a**), but reduces the level of an APP CTF at about 15 KD in mouse forebrain lysates (**b**). Images shown are representatives of at least three independent experiments. **c**, Human CTFβ in the forebrains of APP-SwInd transgenic mice is identified using the method as described in Fig.2d. CTFβ is immunoprecipitated by an antibody against the C-terminus of APP and detected by western blot analysis using an antibody against amino acids 1-16 of human Aβ (6E10), which reacts with CTFβ but not CTFα (regions of antibody epitopes are shown in Fig. 2a). **d**, 5 repeated experiments as shown in panel **c** were quantified by densitometry. For each experiment, the value from PTPσ deficient sample was normalized to the value from the sample with wild type PTPσ. **e**, Representative images of Aβ immunofluorescent staining (with 6E10) in the hippocampus of 15-month old TgAPP-SwInd mice. Arrows point to Aβ deposits. Scale bars, 50 μm. **f**, Aβ immunofluorescent staining in the hippocampus of 15-month old TgAPP-SwInd mice, as shown in panel **e**, was quantified using ImageJ. APP-SwInd(+)PTPσ(+/+), n=7; APP-SwInd(+)PTPσ(-/-), n=8. The mean value of APP-SwInd(+)PTPσ(-/-) samples was normalized to that of APP-SwInd(+)PTPσ(+/+) samples. All error bars, SEM. All *p* values, Student's *t* test, 2-tailed.

Figure 3. Lower affinity between BACE1 and APP in PTPσ-deficient brains.

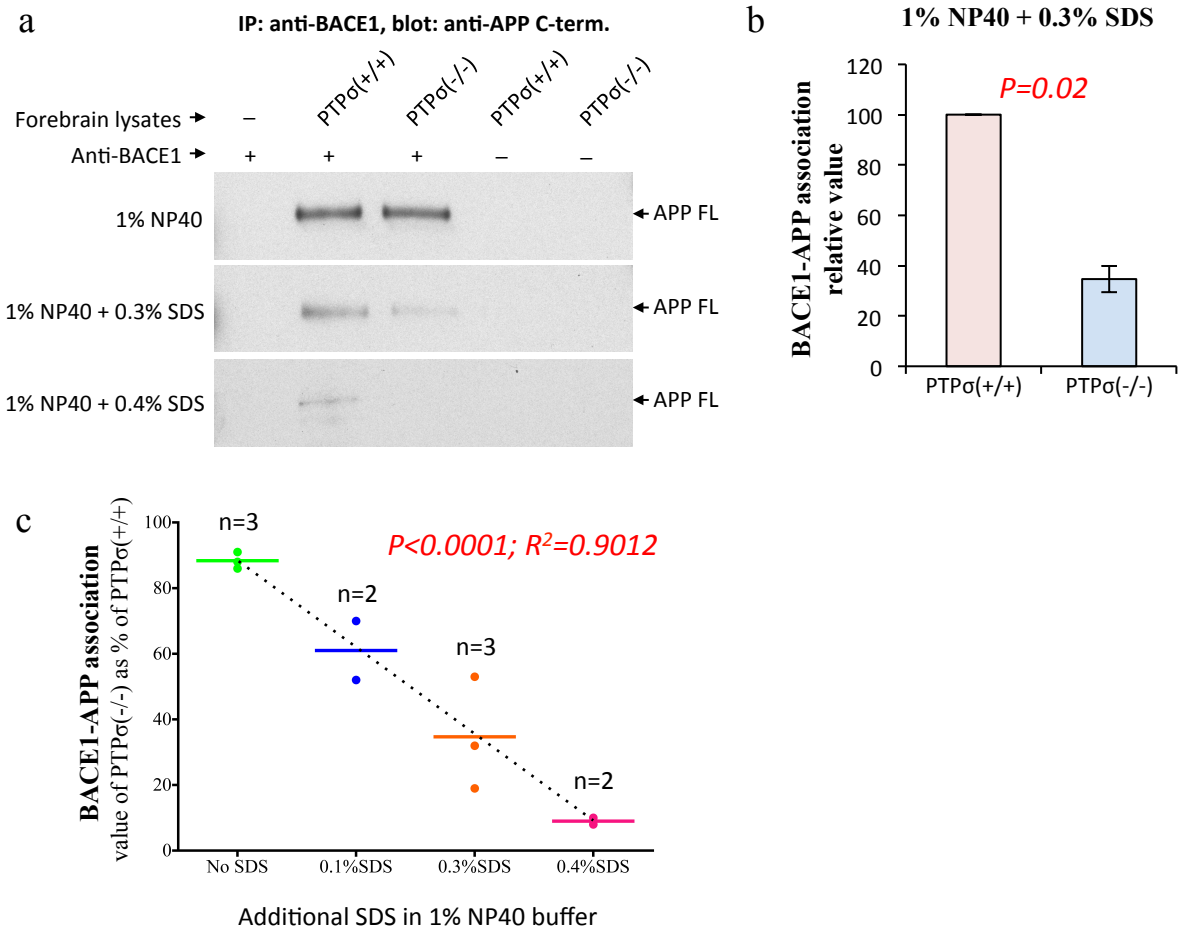

Figure 3. Lower affinity between BACE1 and APP in PTPσ-deficient brains. a, Co-immunoprecipitation experiments show nearly equal BACE1-APP association in wild type and PTPσ-deficient mouse brains under mild detergent condition (1% NP40). However, in PTPσ-deficient brains, BACE1-APP association detected by co-immunoprecipitation is more vulnerable to increased detergent stringency as compared to that in wild type brains. Panels of blots show full length APP (APP FL) pulled down with an anti-BACE1 antibody from mouse forebrain lysates. NP40, Nonidet P-40, non-ionic detergent. SDS, Sodium dodecyl sulfate, ionic detergent. **b**, Co-immunoprecipitation under buffer condition with 1% NP40 and 0.3% SDS, as shown in the middle panel of **a**, were repeated three times. Each experiment was quantified by densitometry, and the value from PTPσ-deficient sample was calculated as a percentage of that from the wild type sample (also shown as orange points in **c**). Error bar, SEM. *p* value, Student's *t* test, 2-tailed. **c**, Co-immunoprecipitation experiments were repeated under each detergent condition. The percentage values shown in dots are derived using the same method as in **b**. Bars represent means. Increasingly stringent buffer conditions manifest a lower BACE1-APP affinity in PTPσ-deficient brains. *p* value and R^2, linear regression.

Figure 4. PTPσ does not generically modulate β- and γ- secretases.

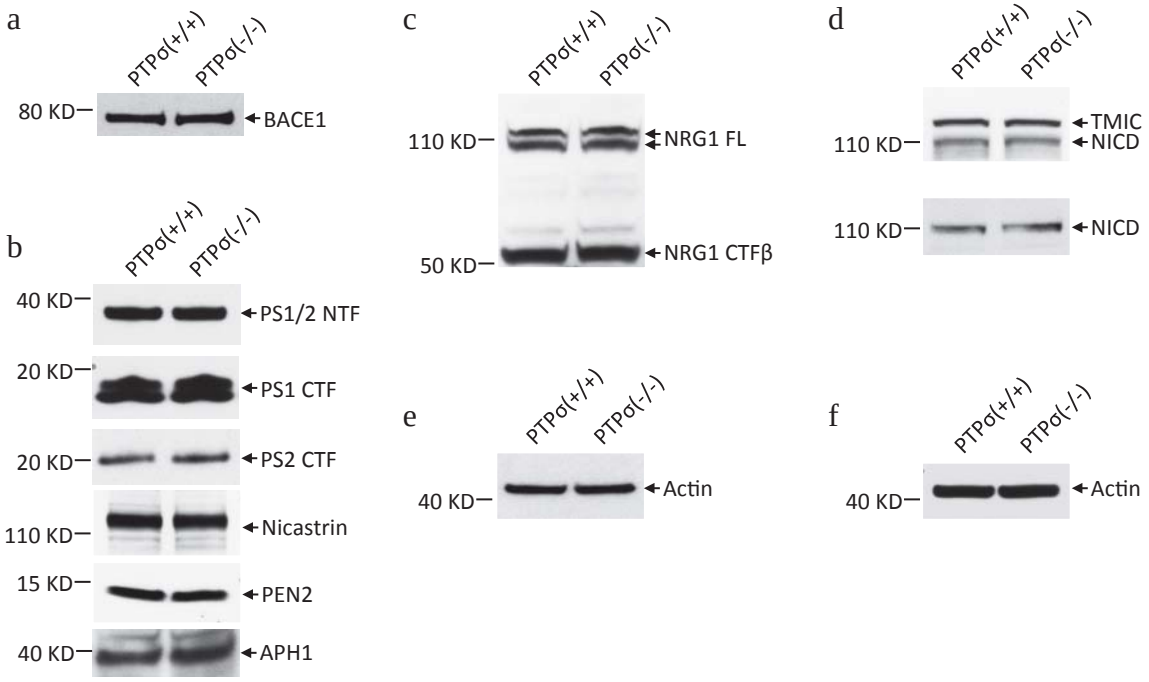

Figure 4. PTPσ does not generically modulate β− and γ− secretases. Neither expression levels of the secretases or their activities on other major substrates are affected by PTPσ depletion. Mouse forebrain lysates with or without PTPσ were analyzed by western blot. **a** and **b**, PTPσ deficiency does not change expression level of BACE1 (**a**) or γ-secretase subunits (**b**). Presenilin1 and 2 (PS1/2) are the catalytic subunits of γ-secretase, which are processed into N-terminal and C-terminal fragments (NTF and CTF) in their mature forms. Nicastrin, Presenilin Enhancer 2 (PEN2), and APH1 are other essential subunits of γ-secretase. **c**, PTPσ deficiency does not change the level of Neuregulin1 (NGR1) CTFβ, the C-terminal cleavage product by BACE1. NRG1 FL, full length Neuregulin1. **d**, The level of Notch cleavage product by γ-secretase is not affected by PTPσ deficiency. TMIC, Notch transmembrane/intracellular fragment, which can be cleaved by γ-secretase into a C-terminal intracellular domain NICD (detected by an antibody against Notch C-terminus in the upper panel, and by an antibody specific for γ-secretase cleaved NICD in the lower panel). **e**, Actin loading control for **a** and **c**. **f**, Actin loading control for **b** and **d**. All images shown are representatives of at least three independent experiments. All images shown are representatives of at least three independent experiments.

Extended Data Figure 3. PTPσ deficiency attenuates reactive astrogliosis in APP transgenic mice.

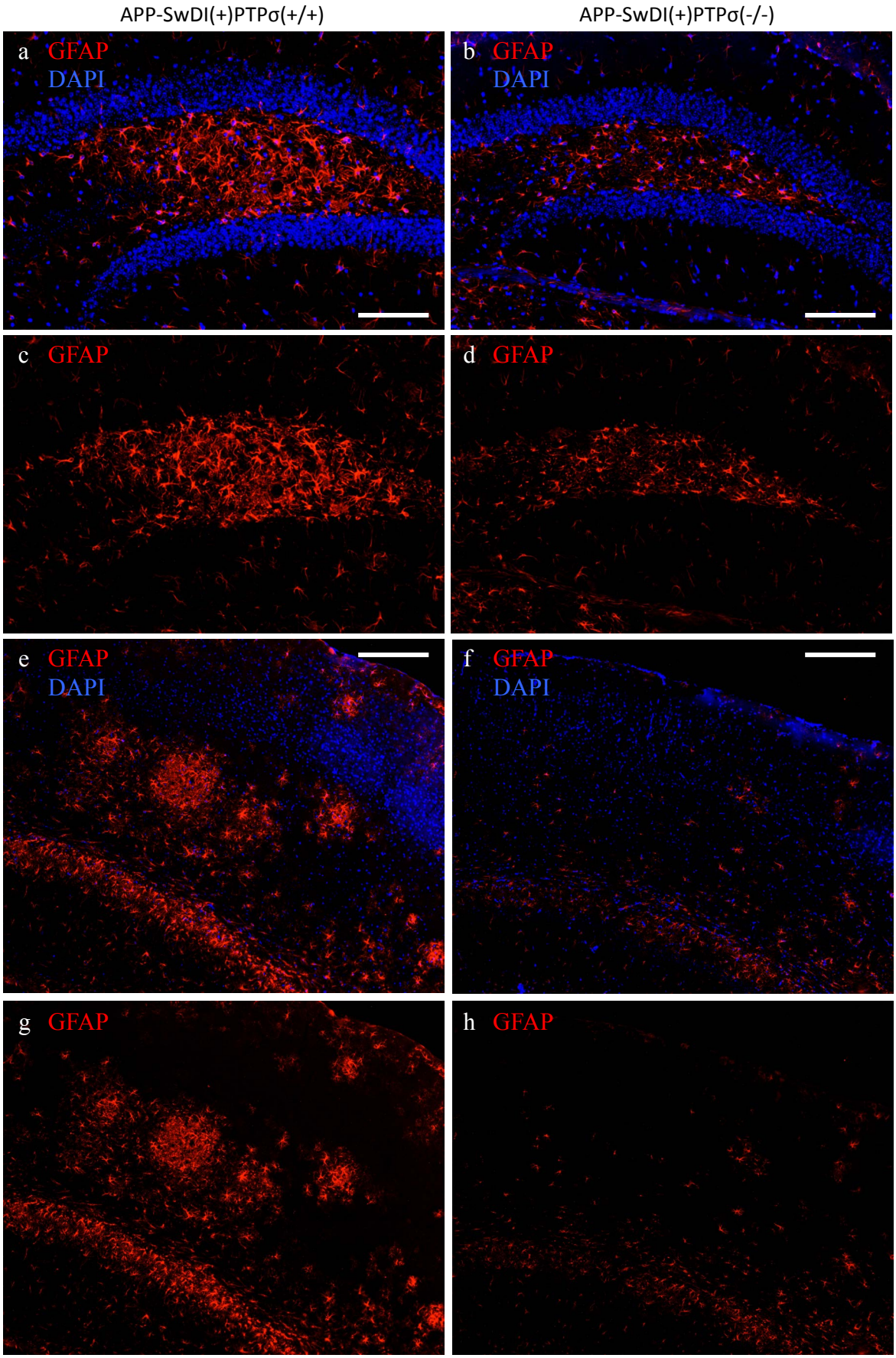

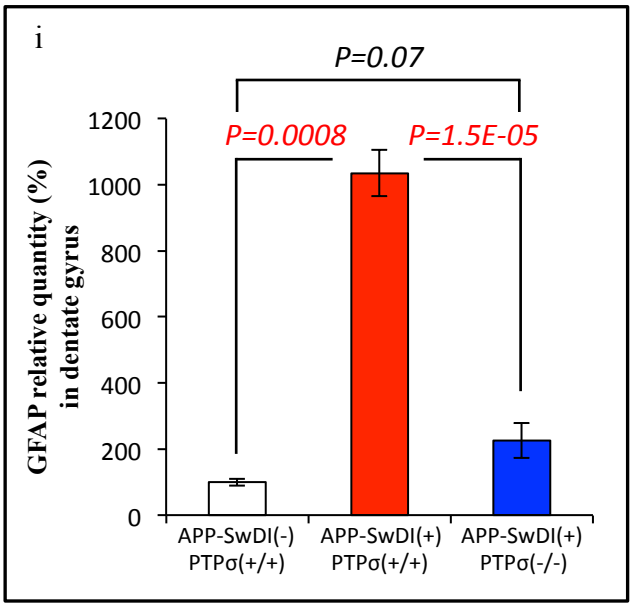

Extended Data Figure 3. PTPσ deficiency attenuates reactive astrogliosis in APP transgenic mice. Expression level of GFAP, a marker of reactive astrocytes, is suppressed in the brains of TgAPP-SwDI mice by PTPσ depletion. Representative images show GFAP (red) and DAPI staining of nuclei (blue) in the brains of 9-month old TgAPP-SwDI mice. **a-d**, Dentate gyrus (DG) of the hippocampus; scale bars, 100 µm. **e-h**, Primary somatosensory cortex; scale bars, 200 µm. **i**, ImageJ quantification of GFAP level in DG hilus from TgAPP-SwDI mice aged between 9 to 11 months. APP-SwDI(-)PTPσ(+/+), non-transgenic wild type littermates (expressing PTPσ but not the human APP transgene). Total integrated density of GFAP in DG hilus was normalized to the area size of the hilus to yield average intensity as shown in the bar graph. Mean value of each group was normalized to that of APP-SwDI(-)PTPσ(+/+) mice (image not shown). APP-SwDI(-)PTPσ(+/+), n=4; APP-SwDI(+)PTPσ(+/+), n=4; APP-SwDI(+)PTPσ(-/-), n=6. All *p* values, Student's *t* test, 2-tailed. Error bars, SEM.

Extended Data Figure 4. PTPσ deficiency protects APP transgenic mice from synaptic loss.

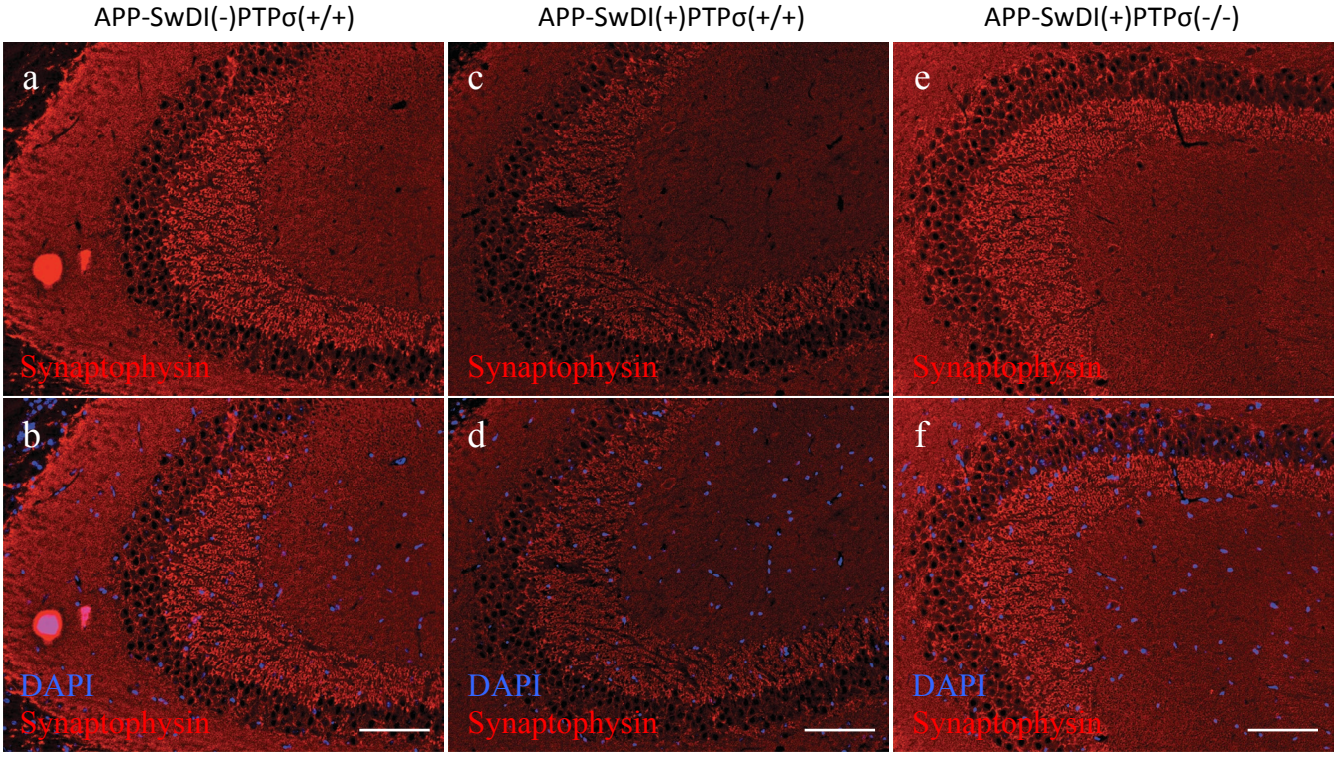

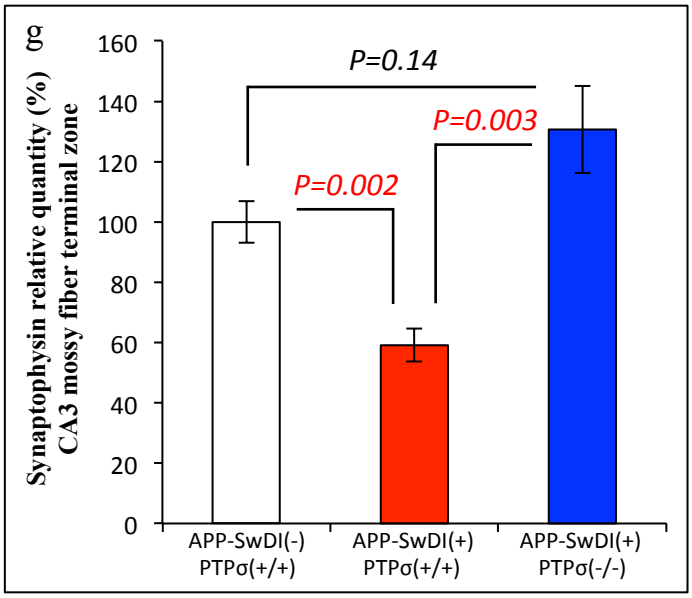

Extended Data Figure 4. PTPσ deficiency protects APP transgenic mice from synaptic loss. Representative images show immunofluorescent staining of presynaptic marker Synaptophysin in the mossy fiber terminal zone of CA3 region. **a-f**, Synaptophysin, red; DAPI, blue. Scale bars, 100 μm. **g**, ImageJ quantification of Synaptophysin expression level in CA3 mossy fiber terminal zone from mice aged between 9 to 11 months. Total integrated density of Synaptophysin in CA3 mossy fiber terminal zone was normalized to the area size to yield average intensity as shown in the bar graph. Mean value of each group was normalized to that of wild type APP-SwDI(-)PTPσ(+/+) mice. APP-SwDI(-)PTPσ(+/+), n=4; APP-SwDI(+)PTPσ(+/+), n=6; APP-SwDI(+)PTPσ(-/-), n=6. All *p* values, Student's *t* test, 2-tailed. Error bars, SEM.

Figure 5. PTPσ deficiency mitigates Tau pathology in TgAPP-SwDI mice.

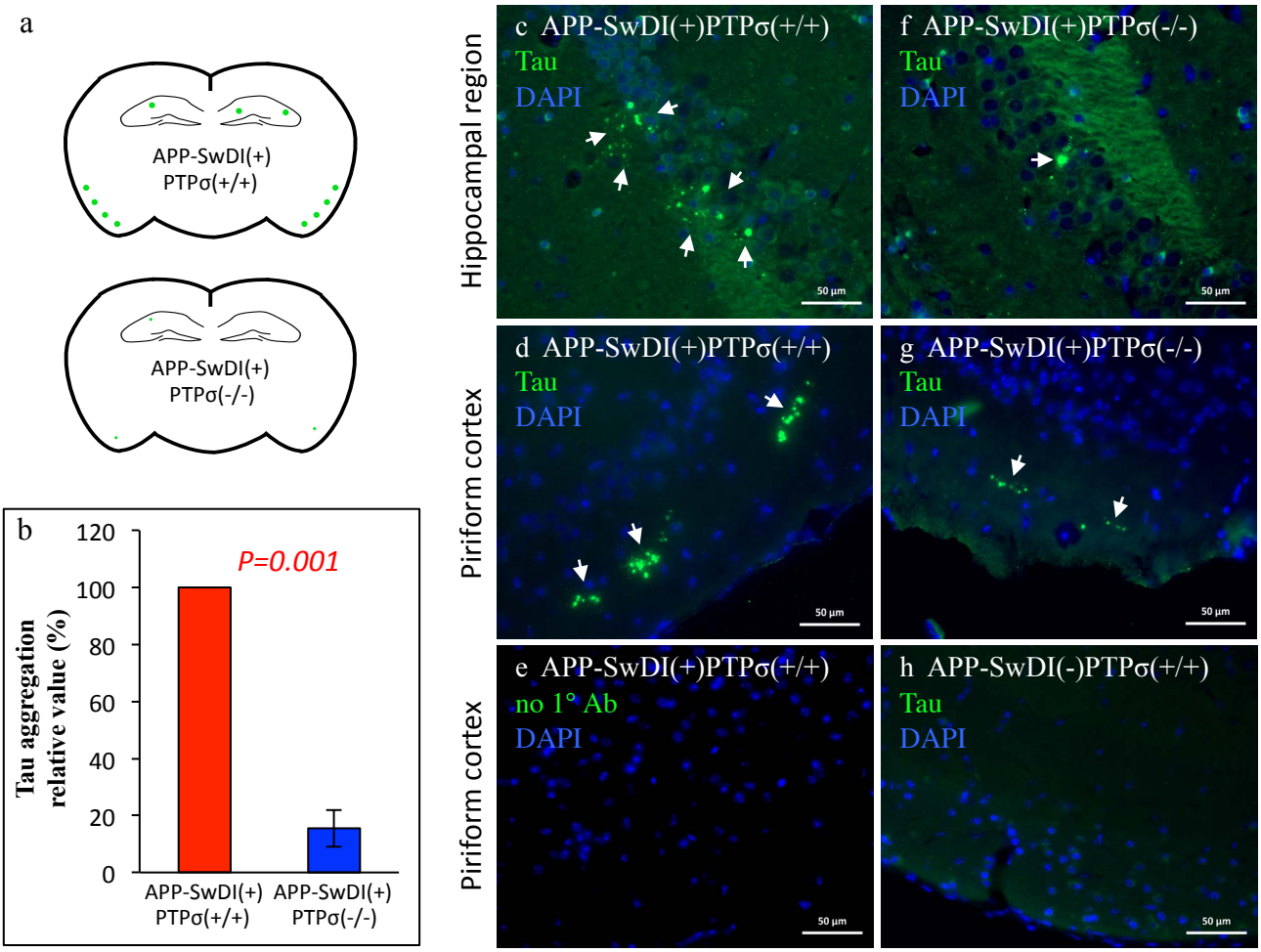

Figure 5. PTPσ deficiency mitigates Tau pathology in TgAPP-SwDI mice. a, Schematic diagram depicting distribution pattern of Tau aggregation (green) detected by immunofluorescent staining using an anti-Tau antibody, in brains of 9 to 11 month-old TgAPP-SwDI transgenic mice. Aggregated Tau is found most prominently in the molecular layer of piriform and entorhinal cortex, and occasionally in hippocampal regions in APP-SwDI(+)PTPσ(+/+) mice. **b**, PTPσ deficiency diminishes Tau aggregation. Bar graph shows quantification of Tau aggregation in coronal brain sections from 4 pairs of age- and sex-matched APP-SwDI(+)PTPσ(+/+) and APP-SwDI(+)PTPσ(-/-) mice of 9 to 11 month-old. For each pair, the value from APP-SwDI(+)PTPσ(-/-) sample is normalized to the value from APP-SwDI(+)PTPσ(+/+) sample. *p* value, Student's *t* test, 2-tailed. Error bar, SEM. **c**, **d**, Representative images of many areas with Tau aggregation in APP-SwDI(+)PTPσ(+/+) brains. **f**, **g**, Representative images of a few areas with Tau aggregation in age-matched APP-SwDI(+)PTPσ(-/-) brains. **c** and **f**, Hippocampal regions. **d-h**, Piriform cortex. **e**, Staining of a section adjacent to **d**, but without primary antibody (no 1° Ab). **h**, no Tau aggregates are detected in aged-matched non-transgenic wild type littermates (expressing PTPσ but not the human APP transgene). Tau, green; DAPI, blue. Arrows points to Tau aggregates. Scale bars, 50 μm.

Extended Data Figure 5. PTPσ deficiency mitigates Tau pathology in TgAPP-SwInd mice.

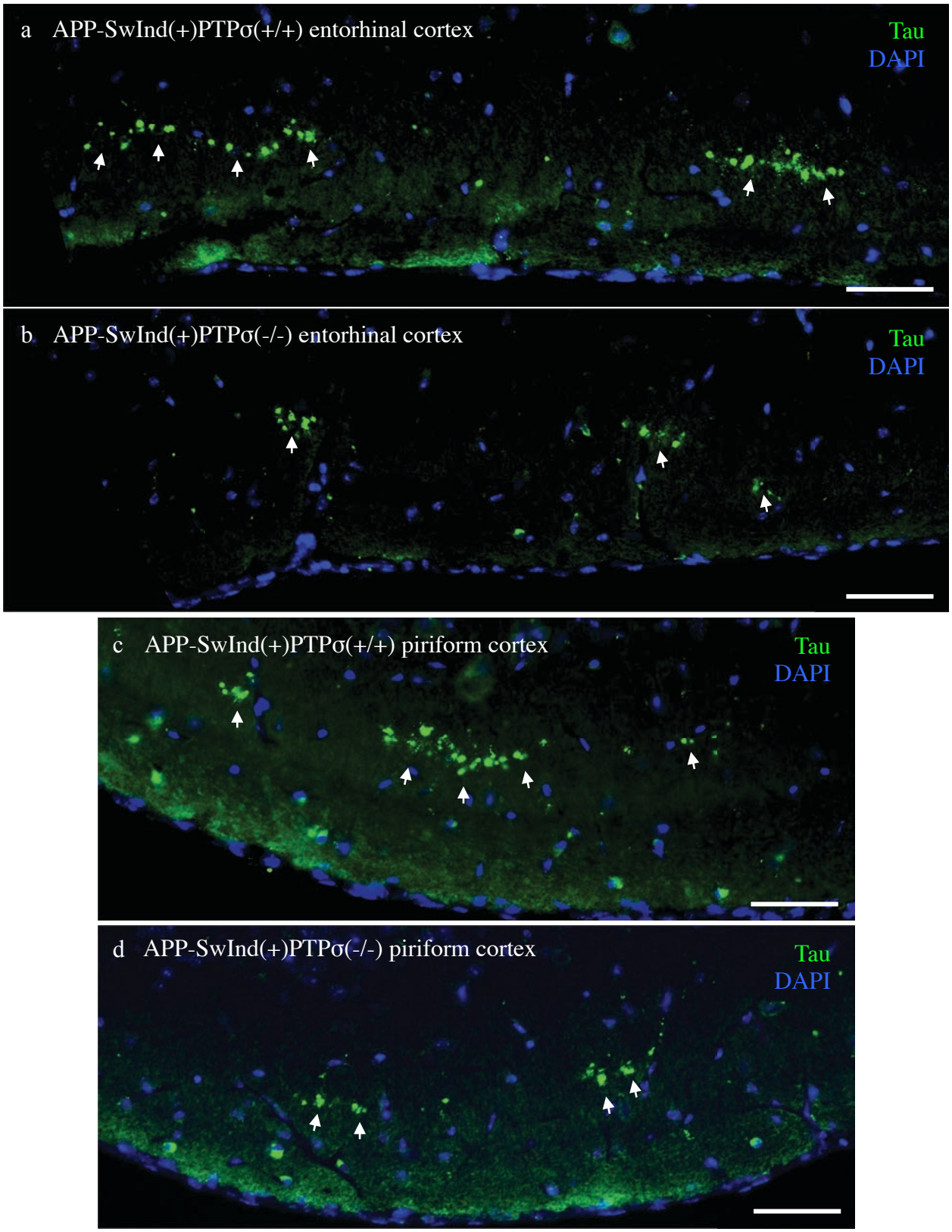

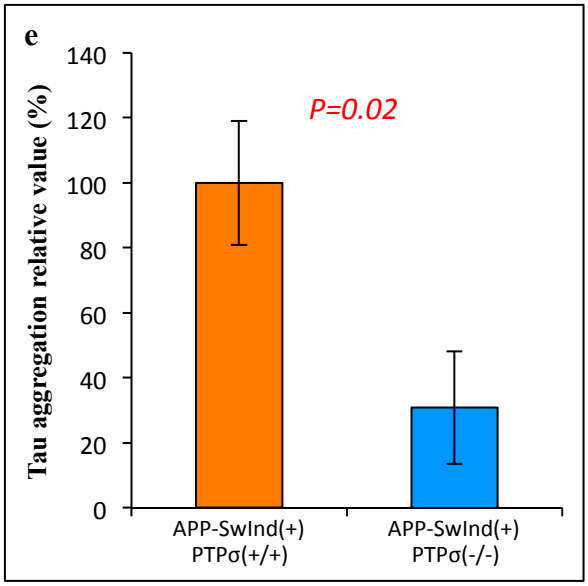

Extended Data Figure 5. PTPσ deficiency mitigates Tau pathology in TgAPP-SwInd mice. Tau aggregation (green) is detected by immunofluorescent staining, using an anti-Tau antibody (as in Fig. 5) in the brains of 15 month-old TgAPP-SwInd transgenic mice. Aggregated Tau is found most prominently in the molecular layer of the entorhrinal (**a**, **b**) and piriform cortex (**c**, **d**), and occasionally in the hippocampal regions (images not shown). **e**, PTPσ deficiency diminishes Tau aggregation as quantified in coronal brain sections from 15 month-old APP-SwInd(+)PTPσ(+/+) (n=7) and APP-SwInd(+)PTPσ(-/-) mice (n=8). The mean value of APP-SwInd(+)PTPσ(-/-) samples is normalized to that of APP-SwInd(+)PTPσ(+/+). *p* value, Student's *t* test, 2-tailed. Error bars, SEM. Tau, green; DAPI, blue. Arrows points to Tau aggregates. Scale bars, 50 µm.

Extended Data Figure 6. Morphology of Tau aggregates found in APP transgenic brains.

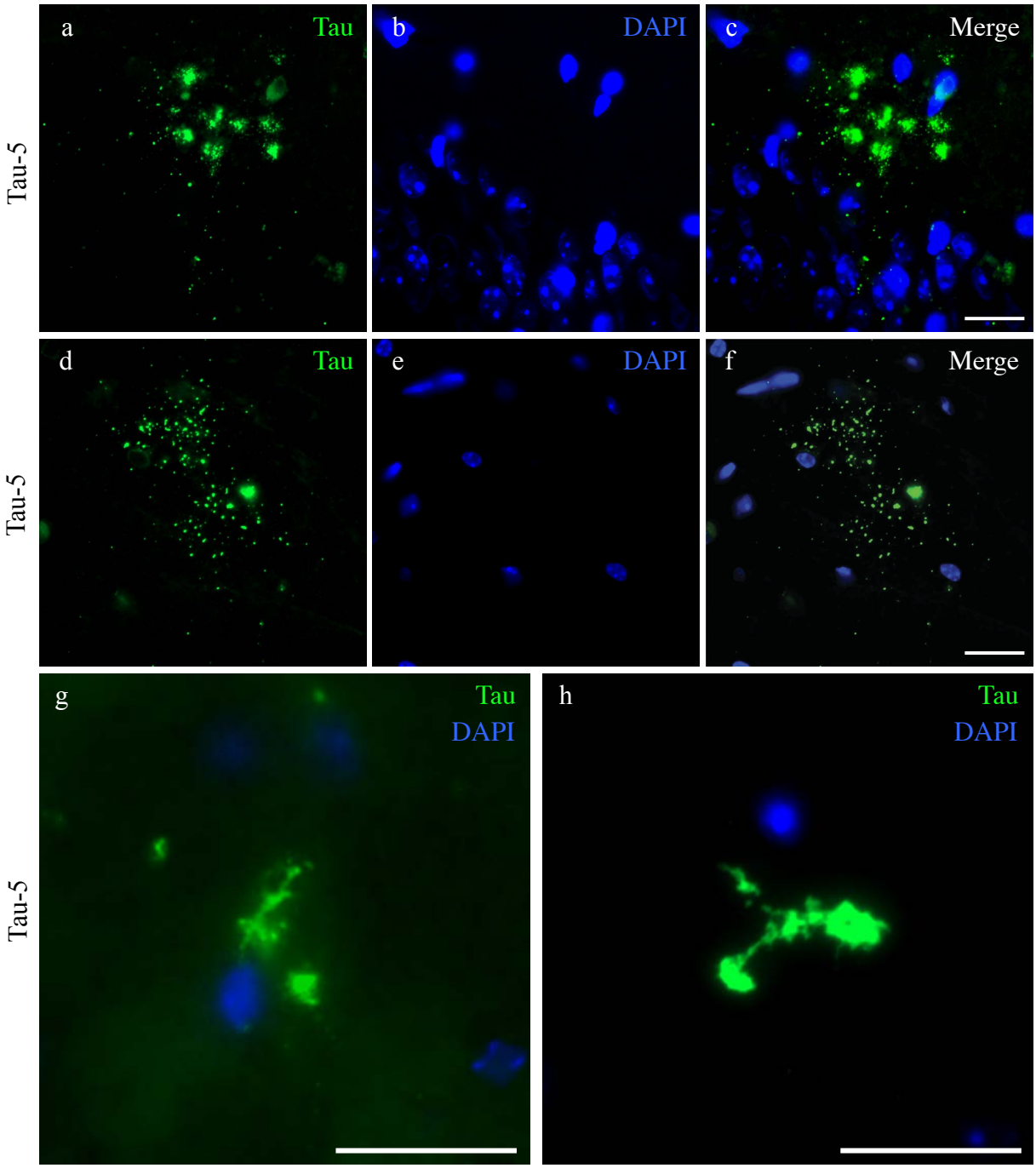

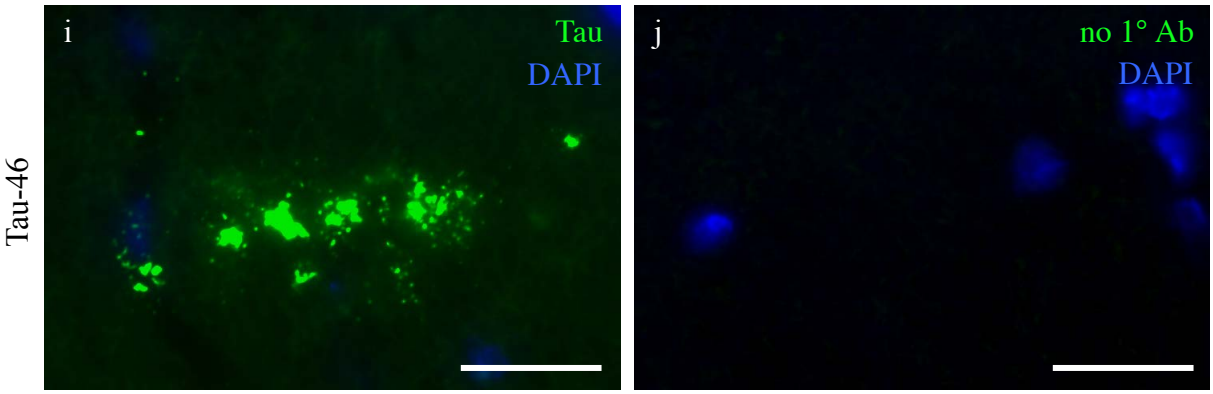

Extended Data Figure 6. Morphology of Tau aggregates found in APP transgenic brains. a-h, Tau aggregation (green) is detected by immunofluorescent staining, using an anti-Tau antibody (Tau-5) against the proline-rich domain of Tau (same as in Fig. 5 and Fig. S5). Tau aggregates in TgAPP-SwDI and TgAPP-SwInd brains show similar morphologies. **a-f**, Many of the Tau aggregates are found in punctate shapes, likely as part of cell debris, in areas that are free of nuclei staining. **g**, **h**, Occasionally the aggregates are found in fibrillary structures, probably in degenerated cells before disassembling. **i**, An additional anti-Tau antibody (Tau-46), which recognizes the C-terminus of Tau, detects Tau aggregation in the same pattern as Tau-5. **j**, Image of staining without primary antibody at the same location of the Tau aggregates in the section adjacent to **i**. Both these antibodies recognize Tau regardless of its phosphorylation status. Tau, green; DAPI, blue. All scale bars, 20 μm.

Extended Data Figure 7. Tau expression is not affected by PTPσ or human APP transgenes.

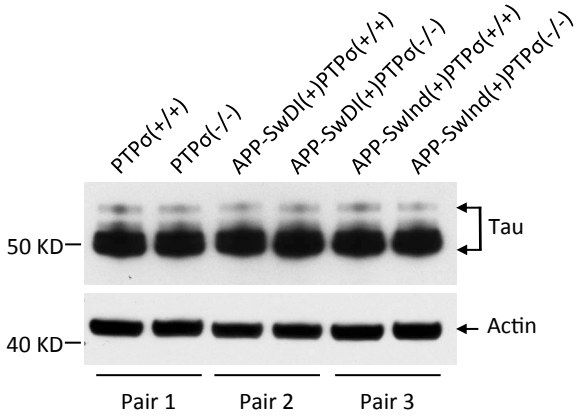

Extended Data Figure 7. Tau expression is not affected by PTPσ or human APP transgenes. Upper panel, total Tau level in brain homogenates. Lower panel, Actin as loading control. Tau protein expression level is not changed by genetic depletion of PTPσ or expression of mutated human APP transgenes. All mice are older than 1 year, and mice in each pair are age- and sex matched. Images shown are representatives of three independent experiments.

Figure 6. PTPσ deficiency rescues behavioral deficits in TgAPP-SwDI mice.

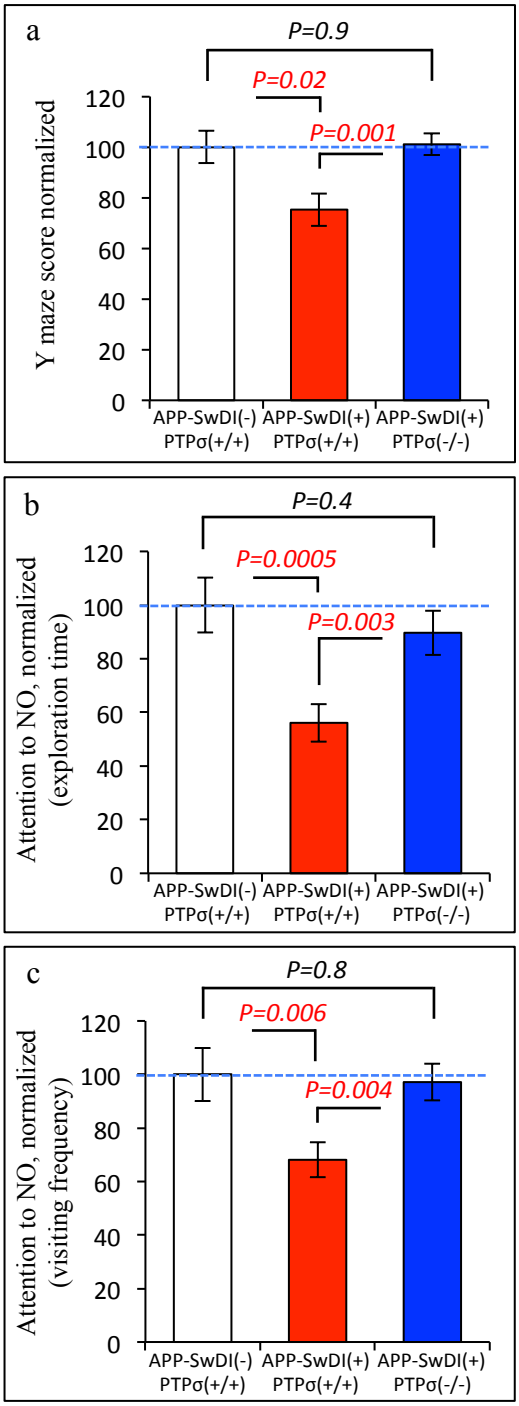

Figure 6. PTPσ deficiency rescues behavioral deficits in TgAPP-SwDI mice. a, In the Y-maze assay, performance of spatial navigation is scored by the percentage of spontaneous alternations among total arm entries. Values are normalized to that of non-transgenic wild type APP-SwDI(-)PTPσ(+/+) mice within the colony. Compared to non-transgenic wild type mice, APP-SwDI(+)PTPσ(+/+) mice show deficit of short-term spatial memory, which is rescued by genetic depletion of PTPσ in APP-SwDI(+)PTPσ(-/-) mice. APP-SwDI(-)PTPσ(+/+), n=23 (18 females and 5 males); APP-SwDI(+)PTPσ(+/+), n=52 (30 females and 22 males); APP-SwDI(+)PTPσ(-/-), n=35 (22 females and 13 males). Ages of all genotype groups are similarly distributed between 4 and 11 months. **b**, **c**, Novel object test. NO, novel object. FO, familiar object. Attention to NO is measured by the ratio of NO exploration to total object exploration (NO+FO) in terms of exploration time (**b**) and visiting frequency (**c**). Values are normalized to that of non-transgenic wild type mice. APP-SwDI(+)PTPσ(+/+) mice showed decreased interest in NO compared to wild type APP-SwDI(-)PTPσ(+/+) mice. The deficit is reversed by PTPσ depletion in APP-SwDI(+)PTPσ(-/-) mice. APP-SwDI(-)PTPσ(+/+), n=28 (19 females and 9 males); APP-SwDI(+)PTPσ(+/+), n=46 (32 females and 14 males); APP-SwDI(+)PTPσ(-/-), n=29 (21 females and 8 males). Ages of all groups are similarly distributed between 4 and 11 months. All *p* values, Student's *t* test, 2-tailed. Error bars, SEM.

Extended Data Figure 8. PTPσ deficiency restores short-term spatial memory in TgAPP-SwDI mice.

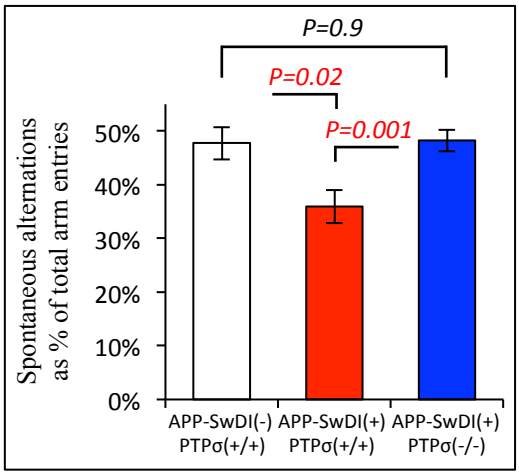

Extended Data Figure 8. PTPσ deficiency restores short-term spatial memory in TgAPP-SwDI mice. In the Y-maze assay, performance of spatial navigation is scored by the percentage of spontaneous alternations among total arm entries. The raw values shown here are before normalization in Fig. 6a. Compared to non-transgenic wild type APP-SwDI(-)PTPσ(+/+)mice, APP-SwDI(+)PTPσ(+/+) mice show deficit of short-term spatial memory, which is rescued by genetic depletion of PTPσ. APP-SwDI(-)PTPσ(+/+), n=23 (18 females and 5 males); APP-SwDI(+)PTPσ(+/+), n=52 (30 females and 22 males); APP-SwDI(+)PTPσ(-/-), n=35 (22 females and 13 males). Ages of all genotype groups are similarly distributed between 4 and 11 months. All *p* values, Student's *t* test, 2-tailed. Error bars, SEM.

Extended Data Figure 9. PTPσ deficiency enhances novelty exploration by TgAPP-SwDI mice.

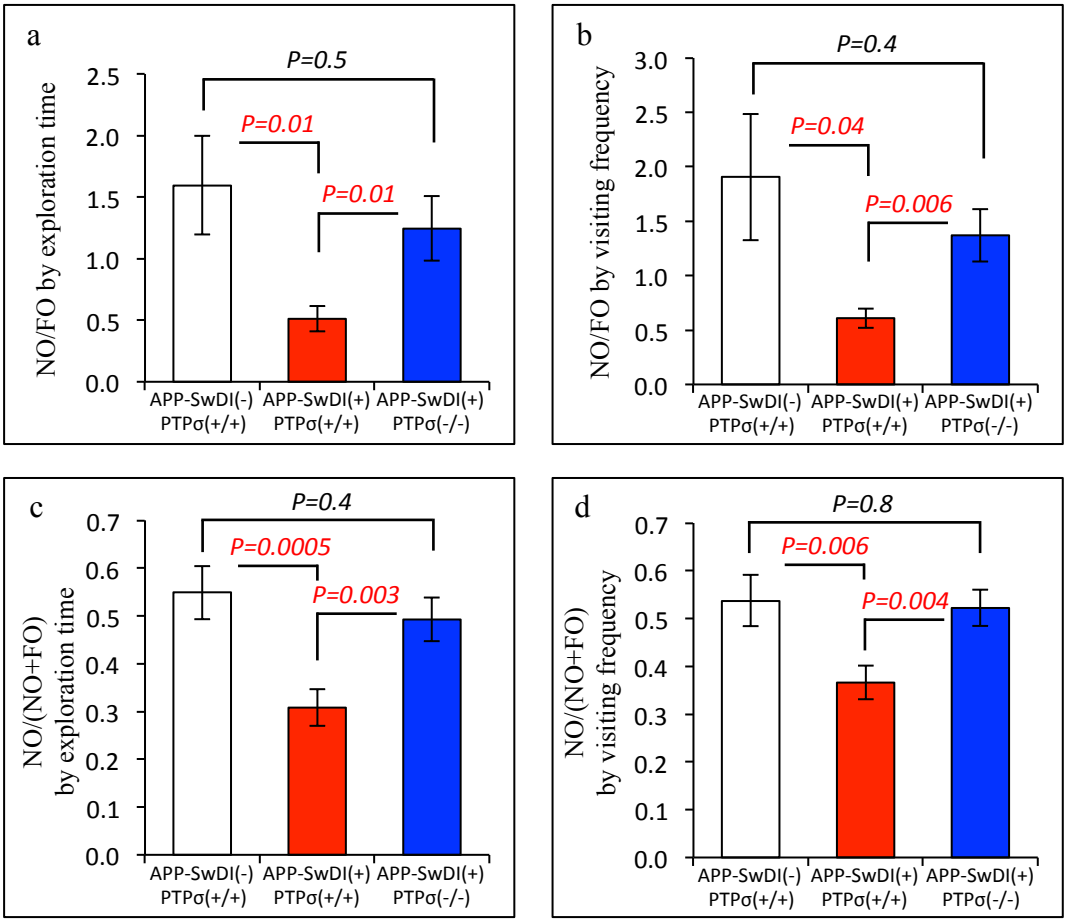

Extended Data Figure 9. PTPσ deficiency enhances novelty exploration by TgAPP-SwDI mice. NO, novel object. FO, familiar object. **a** and **b**, In novel object test, NO preference is measured by the ratio between NO and FO exploration, where NO/FO >1 indicates preference for NO. **c** and **d,** Attention to NO is additionally measured by the discrimination index, NO/(NO+FO), the ratio of NO exploration to total object exploration (NO+FO). The raw values shown here in **c** and **d** are before normalization in Fig. 6b and c. Mice of this colony show a low baseline of the NO/(NO+FO) discrimination index, likely inherited from their parental Balb/c line. For non-transgenic wild type APP-SwDI(-)PTPσ(+/+) mice, the discrimination index is slightly above 0.5 (chance value), similar to what was previously reported for the Balb/c wild type mice [27]. Thus, a sole measurement of the discrimination index may not reveal the preference for NO as does the NO/FO ratio. Although not as sensitive in measuring object preference, the NO/(NO+FO) index is most commonly used as it provides a normalization of the NO exploration to total object exploration activity. While each has its own advantage and shortcoming, both NO/FO and NO/NO+FO measurements consistently show that the expression of TgAPP-SwDI gene leads to a deficit in attention to the NO, whereas genetic depletion of PTPσ restores novelty exploration to a level close to that of non-transgenic wild type mice. **a** and **c**, measurements in terms of exploration time. **b** and **d**, measurements in terms of visiting frequency. APP-SwDI(-)PTPσ(+/+), n=28 (19 females and 9 males); APP-SwDI(+)PTPσ(+/+), n=46 (32 females and 14 males); APP-SwDI(+)PTPσ(-/-), n=29 (21 females and 8 males). Ages of all groups are similarly distributed between 4 and 11 months. All *p* values, Student's *t* test, 2-tailed. Error bars, SEM.

Extended Data Figure 10. PTPσ deficiency improves behavioral performance of TgAPP-SwInd mice.

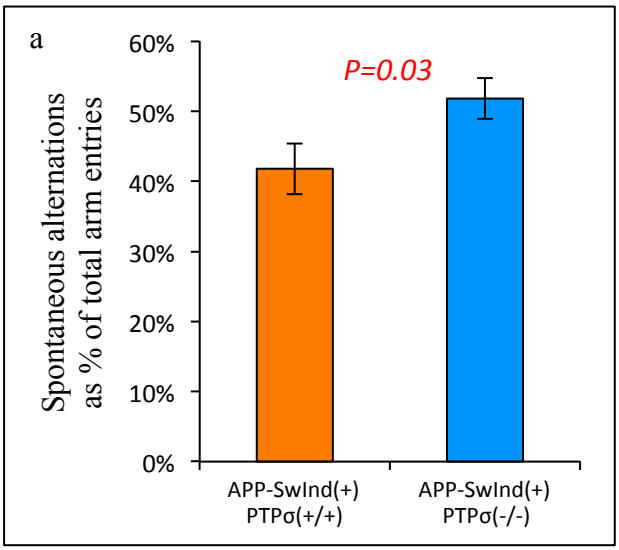

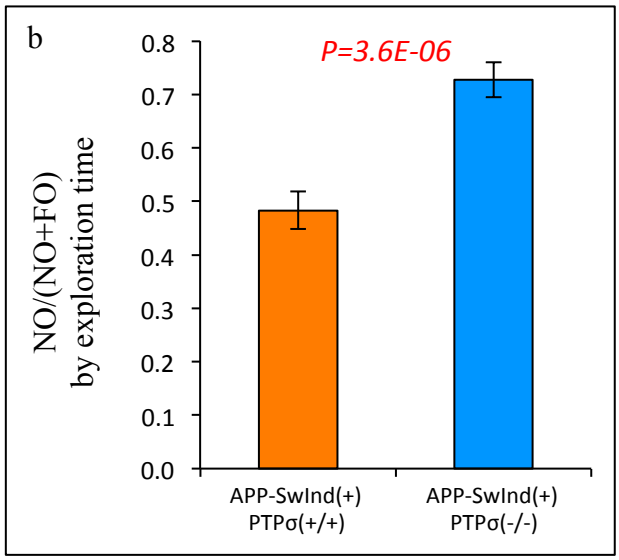

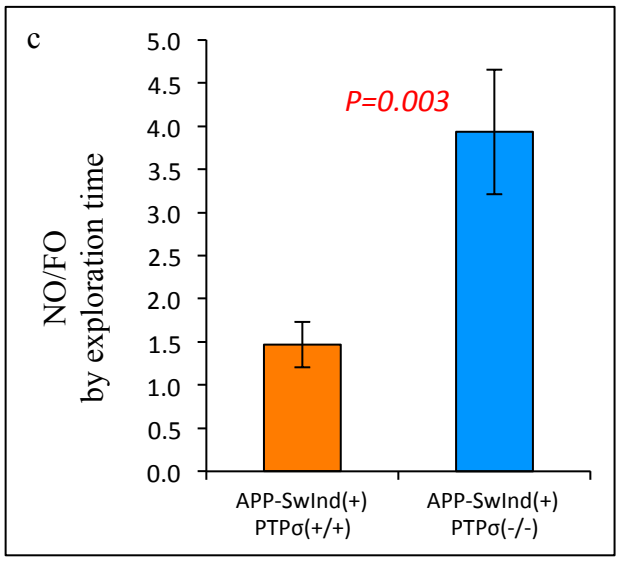

Extended Data Figure 10. PTPσ deficiency improves behavioral performance of TgAPP-SwInd mice. a, Performance of spatial navigation is scored by the percentage of spontaneous alternations among total arm entries in the Y-maze assay. Compared to APP-SwInd(+)PTPσ(+/+) mice, APP-SwInd(+)PTPσ(-/-) mice showed improved short-term spatial memory. APP-SwInd(+)PTPσ(+/+), n=40 (20 females and 20 males); APP-SwInd(+)PTPσ(-/-), n=18 (9 females and 9 males). Ages of both genotype groups are similarly distributed between 4 and 11 months. **b**, **c**, Novel object test. NO, novel object. FO, familiar object. NO preference is measured by the ratio of NO exploration time to total object exploration time (**b**) and the ratio of NO exploration time to FO exploration time (**c**). PTPσ depletion significantly improves novelty preference in these transgenic mice. APP-SwInd(+)PTPσ(+/+), n=43 (21 females and 22 males) ; APP-SwInd(+)PTPσ(-/-), n=24 (10 females and 14 males). Ages of both groups are similarly distributed between 5 and 15 months. All *p* values, Student's *t* test, 2-tailed. Error bars, SEM.